CHALMERS
UNIVERSITY OF TECHNOLOGY

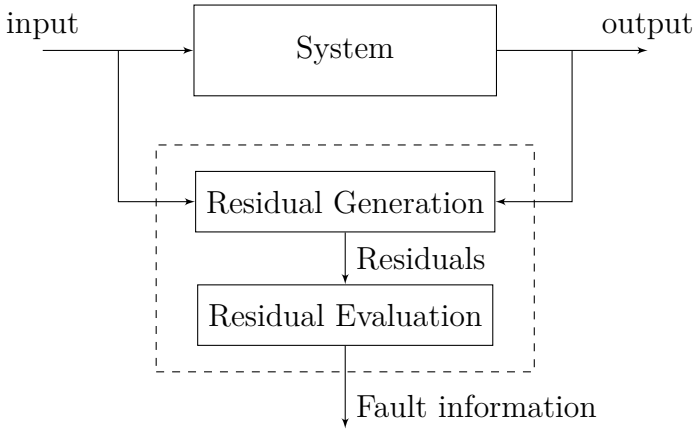

Fault Detection and Isolation in Traction Voltage System

Evaluation of Plausibility Check and Model-Based Approaches

Master's thesis in Systems, Control and Mechatronics

Daniel Hansson & Adam Josefsson

Department of Electrical Engineering
CHALMERS UNIVERSITY OF TECHNOLOGY
Gothenburg, Sweden 2018

Master's thesis 2018:EENX30

Fault Detection and Isolation in Traction Voltage System

Evaluation of Plausibility Check and Model-Based Approaches

DANIEL HANSSON
ADAM JOSEFSSON

CHALMERS
UNIVERSITY OF TECHNOLOGY

Department of Electrical Engineering
Division of Systems and Control
Chalmers University of Technology
Gothenburg, Sweden 2018

Fault Detection and Isolation in Traction Voltage System
Evaluation of Plausibility Check and Model-Based Approaches
DANIEL HANSSON
ADAM JOSEFSSON

Supervisor: Johan Björk-Svensson, Volvo GTT
Examiner: Balázs Kulcsár, Department of Electrical Engineering

Master's Thesis 2018:EENX30
Department of Electrical Engineering
Division of Systems and Control
Chalmers University of Technology
SE-412 96 Gothenburg
Telephone +46 31 772 1000

Cover: General fault detection and isolation scheme.

Fault Detection and Isolation in Traction Voltage System
Evaluation of Plausibility Check and Model-Based Approaches
DANIEL HANSSON & ADAM JOSEFSSON
Department of Electrical Engineering
Chalmers University of Technology

Abstract

As the complexity of the electrical system increases in full electric vehicles the demand of monitoring the system in purpose of safety and preventive maintenance increases. In this thesis the purpose is to evaluate methods for fault detection and isolation in the Traction Voltage system of a Volvo full electric vehicle. The two sub-systems under investigation are the circuitry and a lithium-ion battery cell. For the circuitry a Circuit Fault Detector is designed using plausibility check on voltage and current measurements from sensors distributed in the system. The method is evaluated using log data from normal operation of a full electric bus. It was found to perform well using voltage measurements, however when using the current measurements it is found to not capture the dynamics of the system well enough. An investigation is recommended to conclude if it is the sampling frequency or the estimated currents that is degrading the performance of the detector. Improvements can be made by adding sensors where the system lacks today, this would increase coverage in the system and hence fault detection and isolation can be enhanced.

The Battery Cell Detector is implemented using two model-based fault detection methods, Parity Space Approach (PSA) and State Observer Approach using Adaptive Extended Kalman Filter (AEKF). The model used is a second-order Equivalent Circuit Model of a lithium-ion battery cell. The methods are evaluated through simulations using Volvo's Global Simulation Program (GSP). The PSA was found to be able to detect faults, however due to relying on a Linear Time Invariant model the method was not able to capture all of the dynamics of the nonlinear battery cell well enough and was thus found unsuitable in its current form. The AEKF was found to perform well in both detecting faults and estimating state, but with a potential weakness of high computational complexity when implemented in a real vehicle. While isolation is not possible in neither method in their current form, potential isolation schemes for future investigation are discussed.

For future work, a survey of potential faults and their effect on the sub-systems should be made. Further evaluation of the Circuit Fault Detector and the AEKF method is recommended by a test implementation in the Traction Voltage System.

Keywords: Traction Voltage System, Battery cell, Lithium-ion battery cell, Full Electric Vehicle, Fault detection and isolation, Plausibility test, Parity Space Approach, State Observer, Adaptive Extended Kalman Filter

Acknowledgements

We would like to thank our supervisor Johan Björk-Svensson and Annika Carlsson for the support, the rest of the electromobility team and all other Volvo employees whom we have asked questions. A special thanks to our supervisor at Chalmers, Balázs Kulcsár, who has help us with his expertise in the subject, as well as encouragement during the project. Finally we are grateful for the opportunity to do our Master thesis at Volvo Group Trucks Technology.

Daniel Hansson & Adam Josefsson, Gothenburg, June 2018

Contents

Acronyms

AEKF Adaptive Extended Kalman Filter.

BP Battery Pack.

CAN Controller Area Network.
CSU Charging Switch Unit.

DC/DC DC-DC Converter.

ECM Equivalent Circuit Model.

FDI Fault Detection and Isolation.
FDR False Detection Rate.
FEV Full Electric Vehicle.

GSP Global Simulation Program.

MDR Missed Detection Rate.
MDS Motor Drive System.

PSA Parity Space Approach.

SoC State of Charge.

TVS Traction Voltage System.

List of Figures

List of Tables

1
Introduction

As the development of electrical commercial vehicles is forth going, the general trend is to increase the power handled by the electrical system in the vehicle. As the complexity of the electrical system is increased the perspective of safety and reliability is becoming of increased importance. The consequences of faults can be serious in terms of run time, system health and economic loss. Therefore fault diagnosis methods is needed to monitor these advanced systems in order to reduce the risk and improve safety and reliability.

Fault diagnosis is a subject that has been developed alongside advanced control theory and in the same pace as computers has gained increased processing power more advanced and powerful methods has seen the light of day. Today these methods are accepted as a powerful tool to solve fault diagnose problems [1]. A traditional method of improving a process reliability is to strengthen individual components such as sensors, controllers or computers. Even if this might be an effective method fault-free behaviour can still not be guaranteed and instead fault detection and isolation are becoming a more vital part of modern advanced systems with a demand of high dependability.

The concept of fault diagnosis is divided into three tasks in a rising order of information; fault detection, fault isolation and fault identification. Fault detection is defined as just detecting an occurrence of a fault in the system, fault isolation is defined as locating the fault and fault identification is the highest level which is defined as determining the type, magnitude and cause of the fault. In this thesis only fault detection and isolation will be considered since deeper knowledge of the specific faults in this system is missing and needs a proper survey before it can be implemented.

This thesis aims at performing and evaluating Fault Detection and Isolation (FDI) methods on Volvo GTT's Traction Voltage System (TVS) in a Full Electric Vehicle (FEV). The TVS is the electrical system connecting the batteries, electric drive, electric motor and electric auxiliaries, also called components. It is a high voltage system consisting of high power components, designed to transport passengers or goods in everyday traffic. As the vehicles are increased in size to enhance the capabilities the TVS also grows in both size and complexity, and since multiple parties are dependent on a constantly working solution faults needs to be found and isolated to optimise run time.

Since the TVS is a large system composed by multiple components and have numerous potential sources for faults, a clear breakdown of the system would be to separate the potential faults introduced by wiring issues, and potential faults introduced by malfunctioning components. This give that this thesis is evaluating methods for two detectors with different purpose. The first detector should perform fault detection on the TVS wiring circuit, and the second detector on one of the components in the system. In this thesis a battery cell is chosen as the component for investigation. To clarify which of the two detectors is discussed the method for finding circuitry faults will be called Circuit Fault Detector, whilst the method for finding component faults will be called Battery Cell Detector.

Different categories of faults can occur in a FEV. Quick and vital faults, for example a short circuit, that would make the vehicle instantly stop. Faults that degrade the intended behaviour but are not critical enough to make the vehicle halt. Lastly, faults that does not affect the normal operation in the short run, but degrade the equipment or components at a higher rate. The faults of interest in this thesis are the second and third alternative. Examples of these fault could, for the circuitry, be an increased voltage drop between the batteries and a component or a current leakage in the system, causing abnormal behaviour during driving. This is also why isolation is important, for a battery cell a sensor fault might lead to over-charging or over-discharging, which potentially could lead to fast degradation. For higher severity as if an internal cell fault is found the system might need to be halted immediately to protect the well being of the battery.

The Circuit Fault Detector is designed in regard to the system at hand using a plausibility test, whilst the Battery Cell Fault Detector is evaluated in regards to previously tested model-based fault detection methods. One method that has shown promising results of monitoring a modern battery is a State Observer Approach using an Adaptive Extended Kalman Filter [2][3][4], this method utilises the power of an state observer capable of handling non-linear models with the Adaptiveness to detect abrupt changes. To perform a valid comparison another well known method in fault diagnosis is chosen to be evaluated. This method is the Parity Space approach, which has proven to be an effective fault detector in many systems [1][5][6]. These two methods will be evaluated against each other in an modern Lithium-Ion battery for full electric vehicles.

The report's structure will be as follows; first in Chapter 2 the concept of FDI and the necessary theory around the subject will be presented followed by the chosen methods. The specific system at hand will have a walk-through for basic understanding and the required models will be presented. In Chapter 3 the implementation and the design of the different methods will be handled, as well as the used data and techniques. In Chapter 4 the results of the implemented methods will be presented with its pros and cons before the discussion takes place in Chapter 5. The thesis will be finished with the conclusions and the answers to the specific issue under investigation.

1.1 Purpose and scope

The purpose of this project is to find and evaluate fault detection and isolation (FDI) methods that can tell if a specified TVS sub-system is deviating from normal operation. It is important to find abnormalities in both safety and preventive maintenance perspectives. Since the project is divided into two separate TVS subsystems the scope will differ.

For the circuitry the scope is to design and evaluate a method capable of detecting, and possibly, isolating the faults caused by the wiring circuit. This shall be done using measurements from already installed sensors measuring voltage and current. Updates and improvements that can be made to the system or method shall be included in the evaluation.

For the battery cell the scope is to evaluate the two model-based methods, investigate what is possible to achieve in regard to fault detection and isolation, and compare the methods to each other. Declare the pros and cons of the methods and which one is most suitable for further research, as well as propose possible improvements to enhance the performance of the method.

1.1.1 Specification of issue under investigation

Circuit Fault Detector

- Is there a suitable method to detect and isolate faults in the circuitry using the measurements already present in the system today?
- What are the key factors to improve abnormality detection?

Battery Cell Fault Detector

- Are the two model-based fault detection methods under investigation suitable to be used for monitoring a lithium-ion battery system?
- What are the strength and weakness of the two methods?

1.2 Limitations

The TVS is a large and complex system and therefore this project needs to be limited to be feasible. This project will focus at detecting longer abnormalities, meaning sub-second transients are not included. The project will in the designing and evaluation of the detectors be dependent on faults, but this thesis is limited to only take the faults presented by Volvo into account and will not make an investigation in more detail.

The project is limited to only evaluate a method for one component in the TVS, the battery cell. To evaluate the battery cell models needs to be included, but the project is limited to use existing models and will not develop new ones. The resources at hand are fault-free logged data from an FEV and Volvo's Global Simulation Program (GSP), no field testing or implementation in a real vehicle will be performed.

2
Theory

In this Chapter the necessary theory for the implemented and evaluated methods are presented. First an introduction to Fault Detection and Isolation followed by a more detailed section of the methods and models used and lastly an short introduction of the Traction Voltage System and an analysis of how the system can behave during faults.

2.1 Introduction to Fault Detection and Isolation

Fault diagnosis consist of a vast number of methods and techniques to achieve the same goal, finding faults. The concept is, as earlier mentioned, defined as three different tasks that provides different information level of the detected fault. Fault Detection and Isolation (FDI) are the most fundamental of these three tasks, where detecting the fault is an absolute must and isolation gives vital information. From here on FDI will only be considered.

A fault is in this context defined as an abnormal condition within the system, that may cause reduced functionality in a unit required for a specific task. A fault may not always lead to a breakdown but usually makes the system deviate from normal operation. There exist numerous types of faults and causes, manufacturing faults, maintenance fault, hardware faults, software faults, to only mention a few and most of them are difficult to find. It is especially hard to design a fault detector method for unknown faults, whereas knowing how faults propagates throughout the system helps in making the method mores sensitive to that particular fault. For isolation of a fault it is usually divided into three categories, sensor faults, actuator fault and process faults. Sensor faults are faults that act on the measurements of a process, actuator faults are changes to the actuator or input of the system and process faults are a fault within a process.

Different techniques of detecting faults exists, the simplest and most common is to monitor a given signal and classifying it as an fault if it reaches a set limit. The drawback of this simple method is the lack of understanding the system depending on operation point, input variations or noise. To include some knowledge of the system a plausibility test can be used where the known physical relationships between the input and output values of the system are used to check if the system is consistent. A plausibility test is usually quite simple and hence limited to what can be achieved in sense of detection or isolation in a complex system. This is possible to overcome

with the help of a mathematical model providing a relationship between the different signals in the system. If the model for the system is known well enough it can be run along side the real system, and it is reasonable to expect that it will follow the systems fault-free behaviour for the same input signals. This can then be used to show a fault if the system and model deviate unexpectedly. The difference between these two measurements are called a residual and provide a check of the consistency in the system. The residual should be zero-valued during normal operation and should diverge from zero if a fault is present in the system. This method is called model-based residual generation and is one of the most powerful tools in FDI. These residuals are the heart in the fault detection methods, and different methods of creating residuals provides different residuals generators. The next step of the FDI process is residual evaluation, which is the decision logic that determine if a fault is present in the residual, usually using methods of change-detection. This can be done in multiple ways, by the means of limit checking, estimation of mean and variance, or hypothesis test such as the χ^2-test [5]. In Figure 2.1 the concept of a FDI method is presented with the underlying parts, residual generation and residual evaluation.

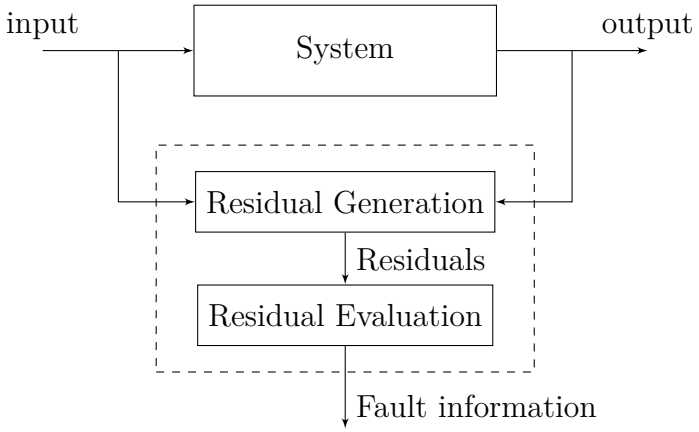

Figure 2.1: Concept idea of fault detection and isolation in a general system with inputs and outputs used by the *Residual Generation* to create a residual used by the *Residual Evaluation* to determine if a fault is present and possibly where it is located.

The residual evaluation is also used to perform fault isolation, i.e. can provide certain information of which error has occurred. This is hard to perform and the system needs certain properties that enables for easier fault isolation, for example a multiple input multiple output system which gives more measuring points and enables for more residuals. The residuals needs to provide information about the faults, and the easiest way is to have multiple residuals that are sensitive or connected to different measurements in the system. This gives that only one of the residuals should react to a certain fault. With this logic it is possible to distinguish where in the system the fault is located if only one of these residuals raise an alarm [1].

2.2 Introduction to systems under investigation

The systems used for FDI are important and below are the relevant systems and models presented.

2.2.1 Traction Voltage System

In this section the system under consideration will be presented, namely the Traction Voltage System (TVS) in the Full Electric Vehicle (FEV) *City Bus Gen 1*, which can be seen in Appendix A under Figure A.1 with the relevant measuring points in the system. The TVS is the electrical system connecting the Battery Packs (BP), Motor Drive System (MDS), 600 V-to-24 V DC-DC Converter (DC/DC), Charging Switch Unit (CSU) and electric auxiliaries such as heater, air compressor and air condition. Above mentioned units can all communicate over a Controller Area Network (CAN) bus, each with packets containing different information. The information relevant for this project are measurements taken at these specific units.

2.2.1.1 Modelling of circuit faults

Since there is no data to access with known faults, this section includes an analysis of how the system should behave during some certain faults. The faults are based on information given on errors that has occurred in the specific system of investigation. The aim is not to find all possible faults that could lead to this behaviour or investigate all possible faults, it is only to gain as much insight so the Circuit Fault Detector can be designed in regards to the TVS.

The first fault is a loose screw in a junction box, causing an increased voltage drop. The screw has either vibrated loose or has not been tighten properly during installation or service. A poor connection will decrease the conductivity and therefore increase the resistance, this can be compared by connecting an additional resistance in series. The second fault is a current leakage which is a ground fault, that could appear when water or moist is entering the system. This can be compared to a resistance parallel to the loads.

In Figure 2.2 a circuit is presented for the help of deriving the affect of serial faults during driving. The circuit contains two voltage sources with the same electrical potential, a fault resistance R_f and both the wire and internal battery resistance combined as R. α is defined as the ratio of the change in resistance in the circuit by the fault, it is also assumed to be smaller than R. Initially it is assumed that the fault resistance, R_f, is not present, and hence i_1 and i_2 will be equal. Deriving the relationship between these two currents and the voltage U gives how the system behaves if R_f would be larger than zero.

The voltage U_1 can be described as

$$U_1 = U - i_1 \cdot \alpha R, \quad U_1 = U - i_2 \cdot R \tag{2.1}$$

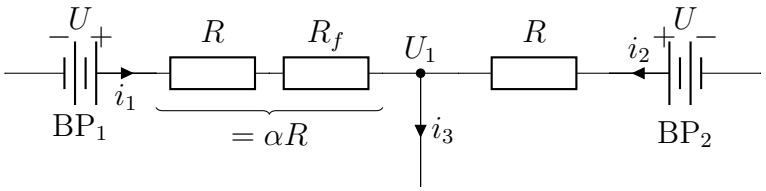

Figure 2.2: An electrical circuit which demonstrates how a serial resistance fault will affect two parallel sources during driving. R is the wire resistance and the internal battery resistance, R_f is the resistance fault. $\alpha = \frac{R+R_f}{R}$.

which gives that this relationship must hold

$$i_1 \cdot \alpha R = i_2 \cdot R. \tag{2.2}$$

By adding Kirchhoff's current law

$$i_1 + i_2 = i_3 \tag{2.3}$$

gives the equation system

$$\begin{bmatrix} \alpha R & -R \\ 1 & 1 \end{bmatrix} \begin{bmatrix} i_1 \\ i_2 \end{bmatrix} = \begin{bmatrix} 0 \\ i_3 \end{bmatrix} \tag{2.4}$$

and by solving this equation system gives

$$\left[\begin{array}{cc|c} \alpha & -1 & 0 \\ 1 & 1 & i_3 \end{array}\right] \Leftrightarrow \left[\begin{array}{cc|c} \alpha+1 & 0 & i_3 \\ 1 & 1 & i_3 \end{array}\right] \Leftrightarrow$$
$$\left[\begin{array}{cc|c} 1 & 0 & \frac{i_3}{\alpha+1} \\ 1 & 1 & i_3 \end{array}\right] \Leftrightarrow \left[\begin{array}{cc|c} 1 & 0 & \frac{i_3}{\alpha+1} \\ 0 & 1 & i_3 - \frac{i_3}{\alpha+1} \end{array}\right] \Leftrightarrow \left[\begin{array}{cc|c} 1 & 0 & \frac{i_3}{\alpha+1} \\ 0 & 1 & i_3\left(1 - \frac{1}{\alpha+1}\right) \end{array}\right].$$

These results can be summarised as

$$\begin{cases} i_1 = \frac{i_3}{\alpha+1} \\ i_2 = i_3\left(1 - \frac{1}{\alpha+1}\right) \end{cases} \tag{2.5}$$

meaning that with an increased fault the currents i_1 will decrease while i_2 will increase. The amount of change depends on the ratio, α, between the fault, R_f, and the combined wire and internal battery resistance, R. The voltage U_1 is also affected by

$$U_1 = U - i_2 \cdot R = U - i_3\left(1 - \frac{1}{\alpha+1}\right) \cdot R \tag{2.6}$$

which will give a lower electrical potential towards the load.

If the system instead is charging the affect of the system will differ since the only source is the charger. In Figure 2.3 the system is presented, with two batteries to charge and with the wire and battery internal resistances R and the fault resistance R_f. With the same equations as in the driving case it is possible conclude that an increased R_f would only give a lower i_1, while i_2 is barely affected since the potential

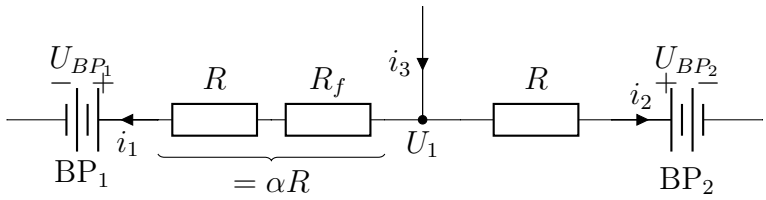

Figure 2.3: An electrical circuit which demonstrates how a serial resistance fault will affect the system during charging. R is the wire resistance and the internal battery resistance, R_f is the resistance fault. $\alpha = \frac{R+R_f}{R}$..

at U_1 is assumed stable from the charger. The voltage drop over BP_1 can still be substantial due to the high currents passing through R and R_f during charging.

This theory includes two possible faults, and since these faults will affect the system differently depending on where it is located a `Simulink`-model was used to simulate the faults. A representation of the electrical system in `Simulink` is shown in Figure 2.4. The potential fault locations, namely R_{f1}, R_{f2}, R_{f3} and R_{f4} can be seen in the figure. In Table 2.1 the system changes can be observed during the faults in both driving and charging. The primary information in the measured signals is how they change compared to each other when a fault occurs and not the specific magnitude, since that differs depending on the fault. Therefore will Table 2.1 only contain the direction of the change.

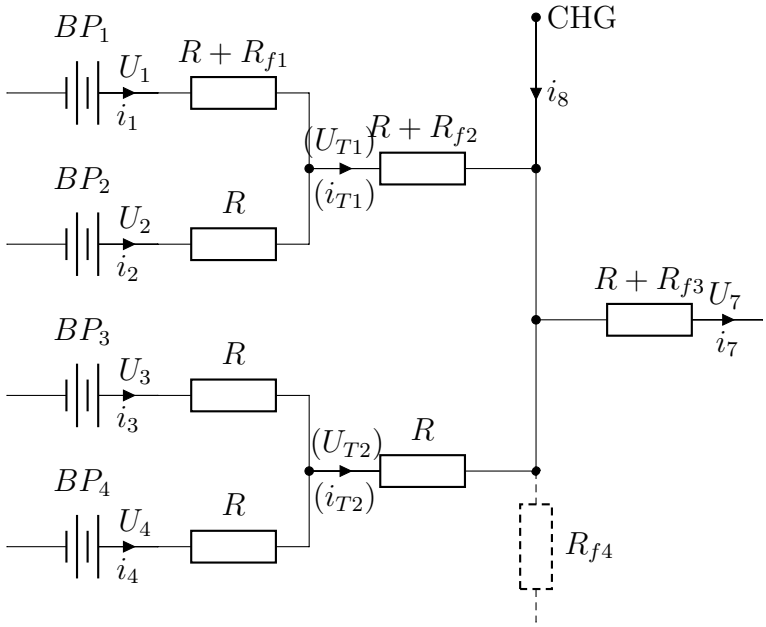

Figure 2.4: A representation of the electrical system with cable resistances, R, and potential faulty serial resistances R_{f1}, R_{f2}, R_{f3} and one faulty parallel resistor of R_{f4}. For simplicity the wire resistance, R, is assumed to be the same throughout the system. All voltages and currents except U_{T1}, U_{T2}, i_{T1} and i_{T2} are accessible in the system, these are included to ease the description of system behaviour.

Table 2.1: The measuring points in Figure 2.4 when a fault has occurred. (+) denotes a small increase, (−) denotes a small decrease, (0) denotes that it is unchanged. Note that the reference for currents are reversed in the charging case compared to the driving case in Figure 2.4. Also note that this is only providing a hint of the direction of the change and does not include any magnitude, two different increases denoted (+) may not be equal in magnitude.

	Driving Case				**Charging case**			
	$R_{f1}\uparrow$	$R_{f2}\uparrow$	$R_{f3}\uparrow$	$R_{f4}\uparrow$	$R_{f1}\uparrow$	$R_{f2}\uparrow$	$R_{f3}\uparrow$	$R_{f4}\uparrow$
i_1	-	-	0	+	-	-	0	0
i_2	+	-	0	+	+	-	0	0
i_3	+	+	0	+	0	0	0	0
i_4	+	+	0	+	0	0	0	0
(i_{T1})	-	-	0	+	-	-	0	0
(i_{T2})	+	+	0	+	0	0	0	0
i_7	0	0	0	0	0	0	0	0
i_8	0	0	0	0	0	-	0	+
U_1	0	0	0	0	-	-	0	0
U_2	0	0	0	0	+	-	0	0
U_3	0	0	0	0	0	0	0	0
U_4	0	0	0	0	0	0	0	0
(U_{T1})	-	0	0	0	-	-	0	0
(U_{T2})	0	0	0	0	0	0	0	0
U_7	-	-	-	0	0	0	-	0

2.2.2 Battery cell

There exists multiple methods on how to model a lithium-ion battery cell, depending on the purpose intended. When only an electrical model is of interest it is possible to use circuit-based models. These circuit-based models are simple and practical since they allow to replace the complex electrochemical process with an Equivalent Circuit Model (ECM) [7]. In Figure 2.5 a second-order ECM is depicted, where U is the terminal voltage when a load is applied to the cell, U_{oc} is the open circuit voltage, U_1 is the voltage over the first transient part, $R_1//C_1$, which captures the fast dynamic such as surface effects and reaction kinetics, U_2 is the voltage over the second transient part which captures the slow dynamic (order of hours), $R_2//C_2$, of the cell such as diffusion processes in electrolyte and active material [8]. R_0 is the internal resistance of the cell and I is the load current.

All of the above mentioned parameters, R_0, R_1, C_1, C_2, R_2 as well as U_{oc}, are dependent on the state of charge (SoC), ageing and cell temperature. The SoC is a percentage of how much of the maximum energy capacity currently is stored in the battery. The parameters corresponding to the transient are all dependent on the load current, which is included in the model. A second order model approximates the transient behaviour in the battery and thus gives an overall more accurate results compared to ECM's of lower order [9][8][3].

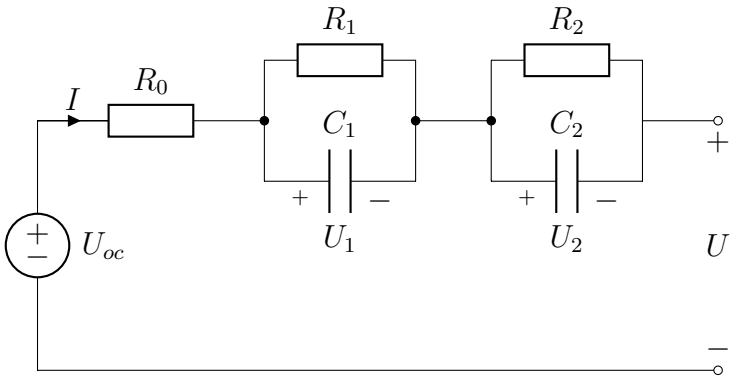

Figure 2.5: A second-order equivalent RC model for an lithium-ion battery cell.

The continuous time dynamics of the battery cell is given in Equation 2.7, where η is the coulombic efficiency, which is dependent on temperature and current. C_{bat} is the capacity in the battery cell, given in ampere hours. The SoC, ageing, temperature and current dependencies of the parameters are omitted for notation simplicity. Discretising Equation 2.7 using zero order hold, the new system presented in Equation 2.8 is achieved, where Δt is the sampling time and k is the time index.

$$\begin{aligned} U(t) &= U_{oc}(SoC(t)) - U_1(t) - U_2(t) - R_0 I(t) \\ \frac{\mathrm{d}U_1(t)}{\mathrm{d}t} &= -\frac{U_1(t)}{R_1 C_1} + \frac{I(t)}{C_1} \\ \frac{\mathrm{d}U_2(t)}{\mathrm{d}t} &= -\frac{U_2(t)}{R_2 C_2} + \frac{I(t)}{C_2} \\ \frac{\mathrm{d}SoC(t)}{\mathrm{d}t} &= -\frac{\eta I(t)}{C_{bat}} \end{aligned} \tag{2.7}$$

$$\begin{aligned} U(k) &= U_{oc}(SoC(k)) - U_1(k) - U_2(k) - R_0 I(k) \\ U_1(k+1) &= \exp\left(-\frac{\Delta t}{R_1 C_1}\right) U_1(k) + R_1 \left(1 - \exp\left(-\frac{\Delta t}{R_1 C_1}\right)\right) I(k) \\ U_2(k+1) &= \exp\left(-\frac{\Delta t}{R_2 C_2}\right) U_2(k) + R_2 \left(1 - \exp\left(-\frac{\Delta t}{R_2 C_2}\right)\right) I(k) \\ SoC(k+1) &= SoC(k) - \frac{\eta \Delta t I(k)}{C_{bat}} \end{aligned} \tag{2.8}$$

The nonlinear state and measurement equations are presented in Equation 2.9, where w_k and v_k are independent zero mean Gaussian noise with covariances Q_k and R_k respectively.

$$\begin{aligned} x_{k+1} &= f(x_k, u_k) + w_k \\ y_k &= h(x_k, u_k) + v_k \end{aligned} \tag{2.9}$$

For the discrete battery model, the state vector is $x_k = [U_1(k),\ U_2(k),\ SoC(k)]^T$,

and f and h can be expressed as,

$$f(x_k, u_k) = \begin{bmatrix} \exp\left(-\frac{\Delta t}{R_1 C_1}\right) U_1(k) + R_1 \left(1 - \exp\left(-\frac{\Delta t}{R_1 C_1}\right)\right) I(k) \\ \exp\left(-\frac{\Delta t}{R_2 C_2}\right) U_2(k) + R_2 \left(1 - \exp\left(-\frac{\Delta t}{R_2 C_2}\right)\right) I(k) \\ SoC(k) - \frac{\eta \Delta t I(k)}{C_{bat}} \end{bmatrix} \tag{2.10}$$

$$h(x_k, u_k) = U_{oc}(SoC(k)) - U_1(k) - U_2(k) - R_0 \cdot I(k)$$

2.2.2.1 Modelling of battery cell faults

Faults that can potentially occur in a battery cell system are sensor and process faults. Sensor faults can occur as effects of manufacturing errors, improper calibration, degradation from usage over long time, or direct trauma such as shocks or vibrations and can manifest themselves in unexpected ways. According to [4], the most common of sensor fault behaviours are bias, drift and scaling of the measurements as well as added noise and hard faults. As for parameter faults the internal resistance of the battery cell can increase due to premature ageing through wear and tear.

2.2.2.2 Local observability and fault detectability

In order to check if faults are theoretically detectable in the battery cell model, local observability for the system is studied. This is checked by confirming that the observability matrix for the model, linearised at normal operating state, is of full rank. Notice that with fault detectability, it is meant; if a fault occurs, independent of its size and type, would it cause a change in the nominal behaviour of the system output [1]. If one can observe all inputs, states and outputs of the model, fault detectability should by the definition presented by S. Ding in [1] be fulfilled. From confirming local observability, global observability is assumed to be fulfilled for all t as well.

2.3 Model-based residual generation

Model-based fault detection is based on the principle of comparing input and outputs from a real system with a nominal one, modelled after physical laws or knowledge of the real system. In Figure 2.6 a general structure for model-based FDI is presented, where residual generation and evaluation is included. In this section two detailed approaches of model-based fault detection are described.

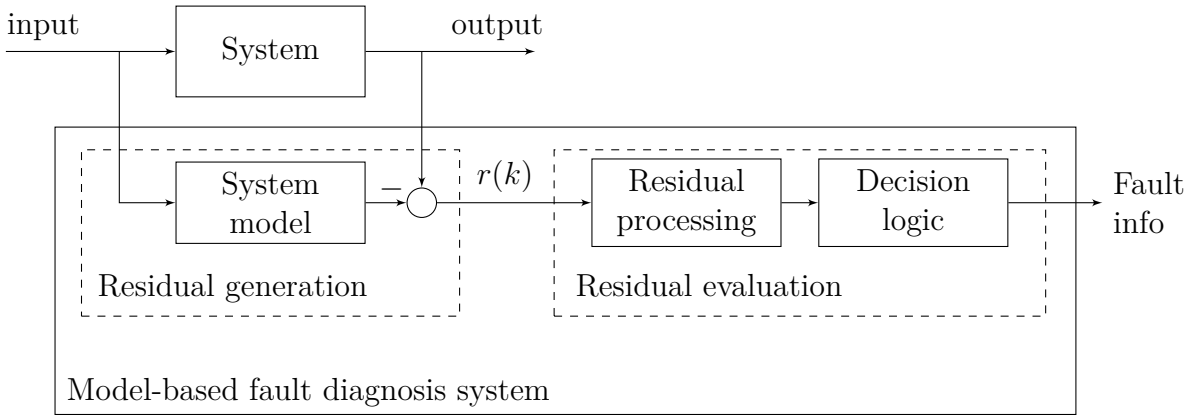

Figure 2.6: Schematic figure of a general Model-based fault diagnosis scheme [1]. The system model is compared with the system to create a residual, which then is evaluated to detect faults.

2.3.1 Parity Space Approach

Parity Space Approach (PSA) is a residual generator that checks the consistency of the measurements in the system. It was first generalised by Chow and Willsky in 1984 and has been well researched since. In this approach the nominal system is assumed to be linear and time invariant, with an known model. This model can be described in multiple forms, such as state-space form, z-transformed input-output model and transfer functions [5][6].

In order to present the parity equations, the system is described on state-space form and the parity equations are considered for discrete-time, since derivations and implementation will be simpler. In Figure 2.7 the PSA is presented, this to give an understanding of the general concept of the method before the mathematical description that follows.

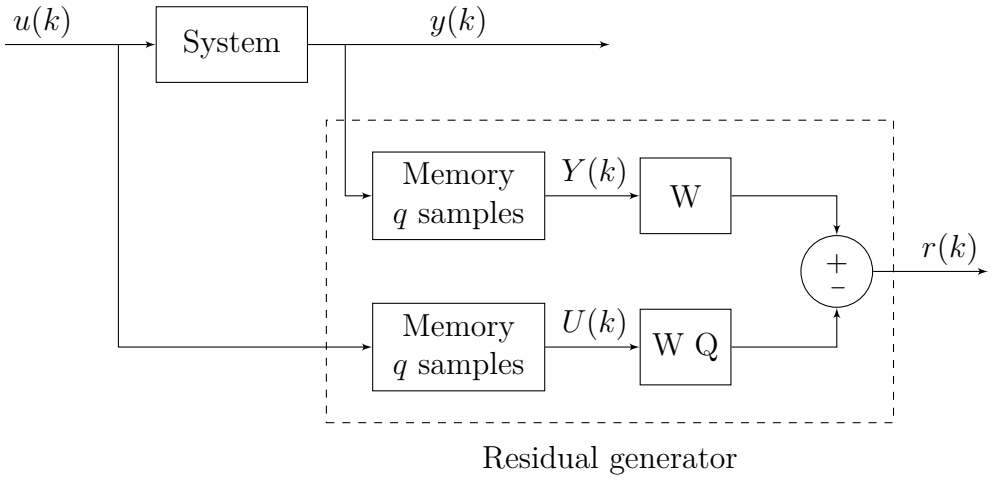

Figure 2.7: Concept of parity space approach with the residual generator [6].

The system is described as

$$x(k+1) = Ax(k) + Bu(k) + w(k) + f_l(k) \tag{2.11}$$

$$y(k) = Cx(k) + Du(k) + v(k) + f_m(k) \tag{2.12}$$

where $w(k)$ and $v(k)$ are independent zero mean Gaussian noise, with covariance Q_k and R_k on input and output respectively. f_l and f_m are additive faults on input and output respectively.

u	process input vector $(p \times 1)$	v	measurement noise vector $(r \times 1)$
x	process state vector $(m \times 1)$	w	input noise vector $(m \times 1)$
y	process output vector $(r \times 1)$	f_l,f_m	fault vectors

For simplification of notation during derivations, the disturbances and faults are dropped from the state-space form, giving

$$x(k+1) = Ax(k) + Bu(k) \tag{2.13}$$

$$y(k) = Cx(k) + Du(k). \tag{2.14}$$

Writing the expression for the output at the next time instant $k+1$, Equation 2.13 is inserted in Equation 2.14, yielding

$$y(k+1) = CAx(k) + CBu(k) + Du(k+1). \tag{2.15}$$

Following this logic the output for time instant $k = q$, is expressed as

$$y(k+q) = CA^q x(k) + CA^{q-1}Bu(k) + ... + CBu(k+q-1) + Du(k+q). \tag{2.16}$$

Here one can observe that the output at time $k = q$ is dependent on the initial state $x(k)$ and the inputs in time window of size $q+1$. Writing out all outputs for this time window and time shifting q samples backwards yields

$$Y(k) = Tx(k-q) + QU(k) \tag{2.17}$$

where

$$Y(k) = \begin{bmatrix} y(k-q) \\ y(k-q+1) \\ \vdots \\ y(k) \end{bmatrix}, \quad U(k) = \begin{bmatrix} u(k-q) \\ u(k-q+1) \\ \vdots \\ u(k) \end{bmatrix} \tag{2.18}$$

and matrices

$$T = \begin{bmatrix} C \\ CA \\ CA^2 \\ \vdots \\ CA^q \end{bmatrix}, \quad Q = \begin{bmatrix} D & 0 & \dots & 0 \\ CB & D & \dots & \\ CAB & CB & & \\ \vdots & \vdots & \ddots & \vdots \\ CA^{q-1}B & CA^{q-2}B & \dots\ CB & D \end{bmatrix} \tag{2.19}$$

where T is the extended observability matrix. Equation 2.17, which is also called the parity relation, describes the input and output relationship of the system with

dependence on the past state vector $x(k-q)$. Since the initial state is unknown, a method is needed to remove this dependency. Equation 2.17 is multiplied with a vector w^T, which fulfils

$$w^T T = 0 \tag{2.20}$$

where $w^T \in \mathbb{R}^{1\times(q+1)r}$. The residuals can now be expressed as

$$r(k) = w^T Y(k) - w^T Q U(k). \tag{2.21}$$

If A is of order m, then $T \in \mathbb{R}^{(q+1)r\times m}$. From Equation 2.20 m elements of w^T is set, the remaining $(q+1)r - m$ can be chosen freely. Further, one can create more residuals by multiplying Equation 2.17 with a matrix W, which contains w^T. W is then determined from following equation

$$WT = 0. \tag{2.22}$$

From Equation 2.22, some elements are determined in order to project the initial state onto the null space. The rest of the elements can again be chosen freely in order for the residuals to have different behaviors, allowing for a better fault isolation or more robust fault detection. In an ideal case the only thing influencing the residuals would be faults, but in real applications both modeling errors and disturbances affect the outcome. One method of designing W is *Structured residuals* also mentioned as *orthogonal parity equation*, where the idea is that the faults do not trigger all residuals. The concept is to make the residual orthogonal to certain faults, this should result in certain patterns appearing during these faults. This is however not straightforward in all cases [5][6]. Multiple other ways of designing W is discussed in Chapter 7.4 *Optimal Selection of Parity Matrices and Vectors* in [1].

The time window, q, can also be chosen differently depending on the system. A larger q gives a more computational heavy system but can in theory provide better fault detection. This is however depending on the system and the guideline is to use at least a higher order than the system at hand and not use a higher order than necessary, i.e. not increase q if there is not clear benefits in terms of fault detection [1].

2.3.2 State Observer Approach using Adaptive Extended Kalman Filter

In this approach to a residual generator, a state observer is designed in order to estimate internal states and output for the use of calculating a residual by adaptive updating of the noise statistics of the filter. In Figure 2.8 the state observer approach is depicted.

The linear discrete time Kalman Filter is a widely used method for state observation, and also as residual generator. Consider the discrete dynamic system presented in Equation 2.13 and 2.14, the purpose of the discrete Kalman filter is to provide state and output estimates on the form,

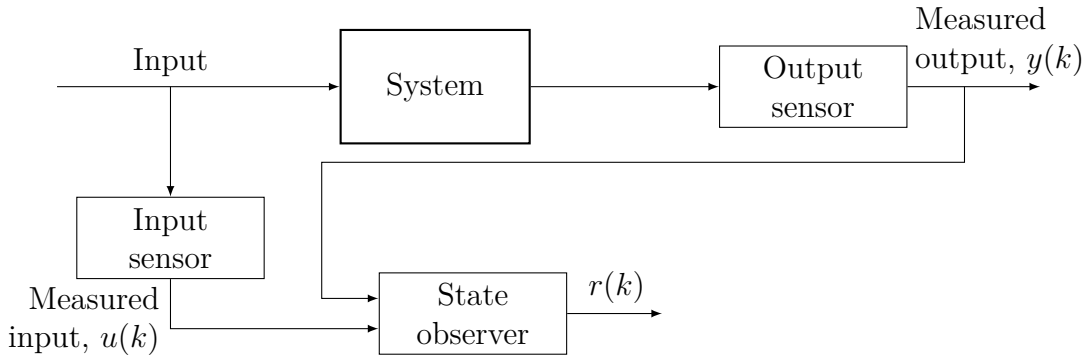

Figure 2.8: Concept of a state observer residual generation approach.

$$\hat{x}(k+1) = A\hat{x}(k) + Bu(k) + K(k)(y(k) - \hat{y}(k)) \tag{2.23}$$

$$\hat{y}(k) = C\hat{x}(k) + Du(k), \tag{2.24}$$

where $\hat{x}$ is the state estimate, $\hat{y}$ is the output estimate and K is the Kalman gain. The filter computes the estimate in a two step process. As a first step, a prediction of the state estimate is performed using the system model, secondly the estimate is updated by a weighted sum with the so called innovation, i.e. the difference between measured output and estimated output. The innovation is in fact the residual, which will be an independent zero mean Gaussian process when no fault is present. When a fault occur, this process will no longer have zero mean.

The state and output estimation of the Kalman Filter is closely connected to the *a priori* information about the process noise and measurement noise, Q_0 and R_0 respectively, where insufficient information will lead to reduced precision or introduction of bias. Wrong *a priori* information will lead to divergence of estimates. An adaptation scheme is therefore added to the filter, where the process and measurement noise covariance, Q_k and R_k, are updated based on the voltage residual covariance. In addition to increasing accuracy of estimation the adaptation will enhance the capabilities of detecting faults. An intuitive explanation of how adaptation enhance fault detection is when abrupt faults occurs, the measurements and estimated output will mismatch and the filter will estimate an increased voltage residual covariance and update process noise covariance and measurement noise covariance accordingly. The filter will then place more trust in either the prediction from the model or the received measurements, since the Kalman gain, K_k is dependent on R_{k-1} and Q_{k-1}. For a more rigorous derivation and explanation of Adaptive Kalman Filter, the reader is advised to [10].

A well known extension of the linear discrete Kalman Filter is the Extended Kalman Filter. The use of an extended version of the regular Kalman Filter, is to capture more of the non-linearities of the system of interest by performing a re-linearisation along the state-trajectory in each iteration of the algorithm. The combination of Extended Kalman Filter and the adaptive property outlined above results in an

Adaptive Extended Kalman Filter (AEKF).

The AEKF is presented in Algorithm 1, where A_k is the Jacobian matrix, C_k is the observation matrix, $\hat{x}_k^-$ is *a priori* state estimate, P_k^- is *a priori* error covariance estimate, $\hat{x}_k^+$ is *a posteriori* state estimate, P_k^+ is *a posteriori* error covariance, K_k is the Kalman gain at time step k, N is the window size of sample covariance calculation, r_k is the residual between the estimated output and measured output at time step k, and $\hat{F}_k$ is the sample covariance of the residual over the window of N samples [3].

Algorithm 1 Adaptive Extended Kalman Filter

$A_k = \frac{\delta f(x_k,u_k)}{\delta x_k}\Big|_{x_k=\hat{x}_k^+,u_k}$, $C_k = \frac{\delta g(x_k,u_k)}{\delta x_k}\Big|_{x_k=\hat{x}_k^-}$

Initialization

For $k = 0$, set $x_0^+ = E[x_0]$, $P_0^+ = E\left[(x_0 - x_0^+)(x_0 - x_0^+)^T\right]$, process noise covariance $\mathbf{Q_0}$ and measurement noise covariance $\mathbf{R_0}$

Computation : For $k = 1, 2, ...$

State estimate time update: $\hat{x}_k^- = f(x_{k-1}^+)$

Error covariance time update: $P_k^- = A_{k-1}P_{k-1}^+A_{k-1}^T + Q_{k-1}$

Kalman gain matrix: $K_k = P_k^-C_k^T(C_kP_k^-C_k^T + R_{k-1})^{-1}$

State estimate measurement update: $\hat{x}_k^+ = \hat{x}_k^- + K_k[y_k - h(\hat{x}_k^-, u_k)]$

Error covariance measurement update: $P_k^+ = (I - K_kC_k)P_k^-$

Update of noise covariance $\mathbf{Q_k}$ and $\mathbf{R_k}$:

For $k = 1, 2, ..., N-1, Q_k = Q_0$ and $R_k = R_0$

For $k >= N$, compute

Residual sequence: $r_k = y_k - h(\hat{x}_k^+, u_k)$

Estimated variance-covariance of residual sequence: $\hat{F}_k = \frac{1}{N}\sum_{j=k-N+1}^{k} r_j r_j^T$

Process noise matrix update: $Q_k = K_k\hat{F}_kK_k^T$

Measurement noise matrix update: $R_k = \hat{F}_k + C_kP_k^+C_k^T$

2.4 Residual evaluation

When the residuals are generated the next step is to evaluate and decide if there is a high possibility of a present fault. This can be done with a few different strategies. A common method is using limit checking with a hypothesis test.

2.4.1 Limit checking

Limit checking is one of the most common and simplest methods of residual evaluation. It includes numerous ways and methods to tune the limits, often called thresholds, to decide if the system residual contains a fault or not. The most simple method is a simple limit check of the absolute values in a monitored variable. Generally, two thresholds are tuned, a maximal value and a minimal value. A usual statement is when

$$Y_{min} \ < \ Y(t) \ < \ Y_{max},$$

which implies a normal operation is present as long as the monitored variable is within the range of the thresholds. These limits are most usually set after training on fault-free data, where it is important to fit the threshold as narrow as possible without the risk of fault detections.

More advanced forms av limit-checking can be achieved by detecting a change in the mean of a larger set of N values. As long as the N values belongs to a known distribution the mean can be monitored and a change can be detected. The problem becomes detecting small changes in a noisy environment, and for this statistical test can be used. One form of statistical test is hypothesis test, which is used for change detection and is described in the next section [5].

2.4.1.1 Hypothesis tests

The objective of a hypothesis test is to make a decision based on observations and the statistical properties of the distribution from which the observation is assumed to belong. The decision is made between two *hypothesises*, which are referred to as the *null-hypothesis*, H^0, and the *alternative hypothesis*, H^1. H^0 represent the fault-free case and H^1 that a fault is present. If the generated residual under test is assumed to have zero mean and the presence of a fault will contribute to a change in mean, then the decision problem can be expressed as

$$D = \begin{cases} H^0, & \text{if } w \leq k \\ H^1, & \text{if } w > k \end{cases} \tag{2.25}$$

where D is the decision, w is the test statistic and k is the threshold. Which test statistic used depend on which type of hypothesis test used, one example is the χ^2*-test* [5].

The χ^2-test assumes that the test statistic belongs to the χ^2-distribution with N degrees of freedom. A statistic follows the χ^2-distribution if it is a sum of squares, in which its elements are uncorrelated, have zero mean and unit variance. The degree of freedom of the statistic, N, is decided by the number of terms in the sum. Once a χ^2-statistic is created it can be compared to a threshold in order to test if the null hypothesis should be accepted or rejected. The threshold for the test can be extracted from a standard χ^2 table or from manually tuning using detector performance as a metric [11].

2.4.2 Detector performance metrics

This section provides a metric that can be used to evaluate the performance of a FDI method.

In statistics two types of errors are often used, Type I error and Type II error which are connected to the null hypothesis, H_0. A Type I error corresponds to the null hypothesis being true, but is rejected. A false positive would in this case be if the detector raised an alarm when there is no fault present. Type II error is the opposite,

when the null hypothesis is false, but erroneously fails to be rejected. In this case it would be when the detector fails to detect a present fault. These two types of errors are useful when evaluating the performance of an FDI method and are called Missed Detection Rate (MDR) and False Detection Rate (FDR). In Table 2.2 there is a summary of the four possible scenarios. [12]

		Null hypothesis is:	
		True	**False**
Decision about null hypothesis:	**Fail to reject**	Correct (True positive)	Type II error (False negative) (MDR)
	Reject	Type I error (False positive) (FDR)	Correct (True negative)

Table 2.2: The relations between truth and falseness of the null hypothesis, the outcomes of the test and which error MDR and FDR are measuring.

To calculate MDR it is defined as

$$\text{MDR} = \frac{\text{Number of rejections}}{\text{Number of faulty samples}}. \tag{2.26}$$

To calculate FDR it is defined as

$$\text{FDR} = \frac{\text{Number of false rejections}}{\text{Number of samples} - \text{Number of faulty samples}}. \tag{2.27}$$

3
Implementation

This chapter will present the design and implementation of the three methods used for fault detection and isolation. First the method for the Circuit Fault Detector is described and then the two methods for the Battery Cell Fault Detector. Lastly the data used for testing the methods is presented and discussed.

3.1 Circuit Fault Detector

This detector is designed as a plausibility check, with the knowledge of the physical relationship between measurements in the TVS system. The system can be described with a static model using Kirchhoff's current and voltage laws, which can be used to create residuals for the system indicating abnormal behaviour.

The detector is implemented using `Matlab` and a basic overview of the program is shown in Algorithm 2. The calculation of the residuals and the residual biases will be discussed in section 3.1.1. The thresholds and how the residuals are evaluated will be discussed in section 3.1.2.

Algorithm 2 Circuit Fault Detector

Initialisation
Residual biases b_1 *etc.*, Thresholds τ_{U1} *etc.*, Kalman Filter settings Q, P
Computation loop : While, k = 1,2,3..
Read measurements from CAN
Filter measurements with a low pass filter (Kalman Filter)
Calculate residuals, $r_{U1}(k) = U_1 - U_5 - b_1$ *etc.*
Evaluate residual, if($r_{U1}(k) > \tau_{U1}$ || $r_{U1}(k) < -\tau_{U1}$) { Raise alarm }
End of loop

The low-pass filtering is performed using two Kalman filters to simplify the implementation, one for the voltage measurements and one for the current measurements with the states U_1 to U_6 and i_1 to i_8 respectively. These states represent the measurement points in Figure A.1 in Appendix. The Kalman filter is chosen since it provides a good, easy to tune low-pass filtering, and is used with a random walk model. During the implementation it became evident that the system measurements properties behave different during stationary charging and driving, and therefore two sets of tuning parameters are provided. More details about the differences of the two cases are explained in Section 4.1. The tuning is done separately for each measurement

to make sure noise and transients are properly removed. In Table 3.1 the tuning for charging and driving is presented.

Table 3.1: Kalman filter tuning for the two cases, driving and stationary charging. The states are U_1 to U_6 and i_1 to i_8 respectively for the two filters in both cases.

Parameter	Setting
Charging	
P_U	I^{8x8}
P_I	I^{6x6}
Q_U	$\mathrm{diag}[0.001, 0.001, 0.001, 0.001, 0.0005, 0.001]$
Q_I	$\mathrm{diag}[0.005, 0.005, 0.005, 0.005, 0.005, 0.0025, 0.05, 0.0035]$
R_U	I^{8x8}
R_I	I^{6x6}
Driving	
P_U	I^{8x8}
P_I	I^{6x6}
Q_U	$\mathrm{diag}[0.01, 0.01, 0.01, 0.01, 0.01, 0.01]$
Q_I	$\mathrm{diag}[0.0001, 0.0001, 0.0001, 0.0001, 0.0001, 0.0025, 0.05, 0.0035]$
R_U	I^{8x8}
R_I	I^{6x6}

3.1.1 Creating residuals

The residual is designed to give information about the system in order to detect and isolate faults. It is hence important to construct residuals containing relevant information about the system.

The construction of the residuals are based on the static relationships of Kirchhoff's voltage and current laws. By analysing how the measuring points should relate to each other in normal operation it is possible to test if Kirchhoff's relationships are fulfilled, if it is not fulfilled a fault is detected. The voltage residuals derived are presented in Table 3.2, the current residuals in Table 3.3 and all residuals are explained below.

According to Kirchhoff's voltage law all components in the system should, in an ideal case, have the same voltage level, therefore it is possible to compare all the voltage measuring points with each other in order to check if any component suffers from a voltage drop. A voltage drop could be caused by a serial resistance fault, as presented earlier in Table 2.1. The first eight voltage residuals, r_{U1} - r_{U8}, are comparing the voltage measurements of each battery with the two components that have voltage sensors, the MDS and the DC/DC. By comparing all batteries with all the components, a redundancy in the residuals is achieved. This means if a fault is located somewhere between the batteries and a component, it should be detected by multiple residuals. If it is not detected by multiple residuals, it is probable to be a false positive. The last five voltage residuals, r_{U9} - r_{U14}, are comparing the batteries

with themselves. These residuals provide information about how the batteries are balanced in comparison to each other, which are intended to be at the same voltage level during normal operation.

For example if residual r_{U1}, r_{U3}, r_{U5} and r_{U7} are detecting a fault it would imply that there is a voltage drop between the MDS and the batteries. The fault is then most likely located near the MDS, since the residuals for the DC/DC does not detect a fault. If instead only r_{U1} is detecting a fault but not r_{U3}, r_{U5} and r_{U7}, it is possible to use residuals r_{U9} - r_{U14} to see if battery pack 1 is deviating. With this methodology it is possible to pinpoint where in the system it is most likely that the cause of the detection is located, even if it is not possible with full certainty to tell exactly what the issue is.

The system consist of sensors from different manufactures that might not be calibrated perfectly and since the voltage in reality is not the same between a voltage source and a voltage load, a new compensation constant is introduced, b_i with $i \in 1...14$, to the voltage residuals. The constant makes it possible to reduce the voltage difference between measuring points of normal operation and hence reduce the threshold for the decision process and be able to find smaller faults. The compensation constant is found by comparing the measured signals and the residuals over time to conclude if there is a constant bias. This compensation constant will also need to be updated over time, since it can change depending on the calibration of the sensors.

Table 3.2: The 14 voltage residuals used, built from the measuring points in the TVS that can be seen in Figure A.1. U correspond to the measuring points and b correspond to the compensation constant to remove the voltage bias in the system.

Voltage residuals:

$$
\begin{aligned}
r_{U1} &= U_1 - U_5 - b_1 \\
r_{U2} &= U_1 - U_6 - b_2 \\
r_{U3} &= U_2 - U_5 - b_3 \\
r_{U4} &= U_2 - U_6 - b_4 \\
r_{U5} &= U_3 - U_5 - b_5 \\
r_{U6} &= U_3 - U_6 - b_6 \\
r_{U7} &= U_4 - U_5 - b_7 \\
r_{U8} &= U_4 - U_6 - b_8 \\
r_{U9} &= U_1 - U_2 - b_9 \\
r_{U10} &= U_1 - U_3 - b_{10} \\
r_{U11} &= U_1 - U_4 - b_{11} \\
r_{U12} &= U_2 - U_3 - b_{12} \\
r_{U13} &= U_2 - U_4 - b_{13} \\
r_{U14} &= U_3 - U_4 - b_{14}
\end{aligned}
$$

The current residuals are based on Kirchhoff's current law, where the first residual, r_{i1}, is designed to compare all current measurements from the sources and the loads

in the system. If there is a difference in the current drawn from the source and current consumed by the loads there is a inconsistency, which is not possible without a fault. Six more residuals, r_{i2} - r_{i7}, are created by comparing the current drawn from the batteries. If the current usage from the batteries diverge a fault could be present, as earlier shown in Table 2.1. Since it is not possible to create more current residuals between different points in the system it is not possible to use the same methodology for isolation as in the voltage case, hence it is not possible to isolate the faults. An example fault is if a parallel resistance is present in the system. It will be detected by r_{i1} as long as the current it is using is large enough to surpass the set threshold for the residual, but it will not be possible to isolate since only one residual is detecting the abnormality.

Table 3.3: The seven current residuals used, built from the measuring points in the TVS that can be seen in Figure A.1.

Current residuals:

$$r_{i1} = i_1 + i_2 + i_3 + i_4 + i_5 + i_6 + i_7 - i_8$$
$$r_{i2} = i_1 - i_2$$
$$r_{i3} = i_1 - i_3$$
$$r_{i4} = i_1 - i_4$$
$$r_{i5} = i_2 - i_3$$
$$r_{i6} = i_2 - i_4$$
$$r_{i7} = i_3 - i_4$$

3.1.2 Evaluation of residuals

The method of evaluating the residuals are chosen to be limit-checking, which simply checks that the residual is within a specified range from zero. The range is specified with two thresholds, one positive and one negative, that in this case are the negation of each other. This creates a range of double the threshold centered around zero.

The threshold is set with help of the training data and the FDR. Each threshold is set and tweaked manually until a reasonably low FDR is reached and finally the threshold is confirmed with the validation data to make sure it is not overfitted. The data used is presented in Section 3.3.1 and the resulting thresholds can be seen in Section 4.1.1 of the Results chapter.

3.2 Battery Cell Fault Detector

In this section the methods for implementing and simulating PSA and AEKF residual generators are first presented. The method for tuning, residual evaluation and how thresholds where set for both approaches will be presented secondly.

3.2.1 Parity Space Approach

The PSA is designed according to the theory presented in Section 2.3.1, but since this method is applied to a nonlinear lithium-ion battery model, the system needs to be linearised. The model is dependent on multiple parameters, such as current, temperature and SoC. The linearisation is performed at an operating point of 23°C, a charging current of 74 A and a SoC of 55%. By using parameters from Volvo's Global Simulation Program (GSP) that matches with the operating point, a linearised model is achieved. The model can be seen in Appendix A.1.

The implementation of the PSA theory is performed in `Simulink` and presented in Figure 3.1. The `Simulink` implementation contains seven different parts, separated with blue backgrounds in the figure. The seven parts are *Input*, *Measurement noise*, *Fault input*, *Fault output*, *Process*, *Output* and *PSA*. These parts are comparable with the previously presented concept figure of the PSA, Figure 2.7, where $u(k)$ is the *Input* block, $y(k)$ is the *Output* block, *System* is the *process* block and the *Residual generator* is the block named *PSA* in `Simulink`.

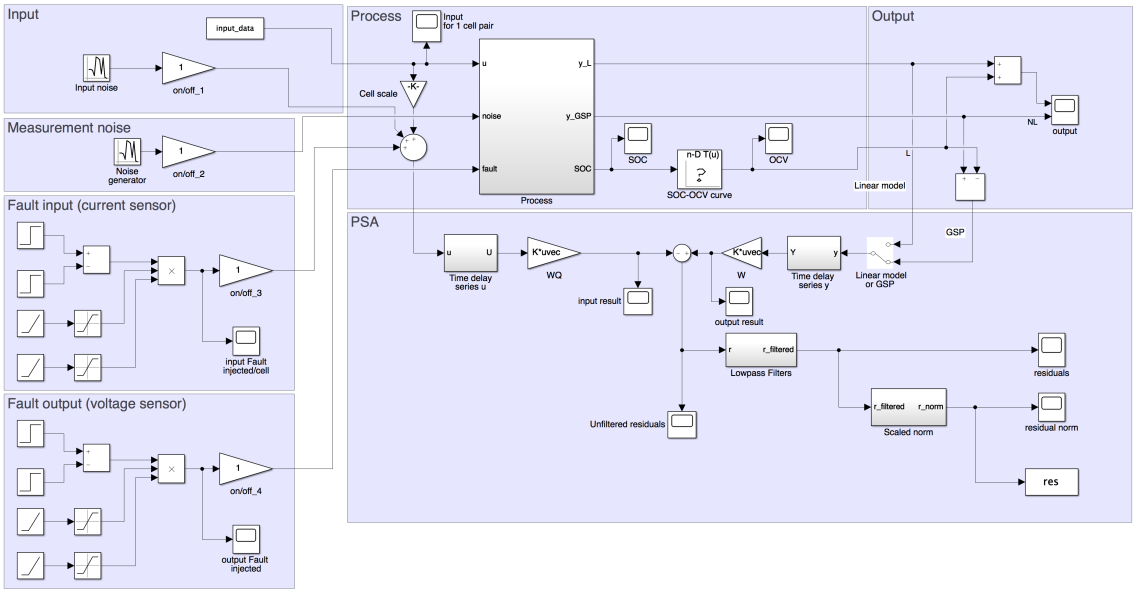

Figure 3.1: Implemenation of PSA in `Simulink` based on the theory presented in Section 2.3.1.

Beyond the concept figure some other features have been implemented to be able to test the implementation and to make it more realistic. The *input* block adds

Gaussian distributed noise to the input current measurements, the *Measurement noise* block adds Gaussian distributed noise to the output voltage measurements. The *Fault input* and the *Fault output* block makes it possible to add faults to the input current sensor and the output voltage sensor respectively.

The *Process* utilises the GSP to simulate a battery cell and provides the process output for the PSA. It does also remove the stationary output from the nonlinear system, so it can be used with the linear PSA system.

The *PSA* block is the heart of the fault detection and contains the same structure as the residual generator in Figure 2.7, with some added functionality. To remove some of the noise in the residual a low-pass filer is implemented, and lastly the norm of the residuals is calculated according to the χ^2 statistics.

3.2.1.1 Tuning of parameters

W has two functionalities, first to project the states to null space and then to create residuals that are sensitive to the faults intended to find. In this implementation W is only used to project the states to null space and thus the freedom of kernel projection is left unexplored. This can be implemented to improve the detection and robustness but is left since it is deemed to be out of the scope to optimally tune the PSA. W is calculated using single value decomposition, and gives

$$W = \begin{bmatrix} 0.0000 & 0.0146 & 0.4312 & 0.8698 & 0.1261 & -0.1217 & 0.1174 & -0.1133 \\ 0.0000 & -0.0153 & -0.4171 & 0.1257 & 0.8783 & 0.1175 & -0.1133 & 0.1094 \\ 0.0000 & 0.0148 & 0.4025 & -0.1213 & 0.1174 & 0.8867 & 0.1094 & -0.1055 \\ 0.0000 & -0.0143 & -0.3884 & 0.1170 & -0.1133 & 0.1094 & 0.8945 & 0.1018 \\ -0.0000 & 0.0138 & 0.3748 & -0.1129 & 0.1094 & -0.1055 & 0.1018 & 0.9017 \end{bmatrix}$$

The time horizon, q, is in the end set to seven and the value is set by trial and error. It was found that no increase of performance was found over this value, and since the computational complexity increases with q it is advantageous to keep it relatively low.

3.2.1.2 Evaluation of residuals

The fault-free samples of the generated residual signals are assumed to be independent zero mean Gaussian with variance corresponding to the measurement noise covariance. By the theory in Section 2.4.1.1 one can then construct a test statistic that follows the χ^2 distribution by taking the sum of squares of the residual signals and normalising with the measurement noise covariance. The test statistic is then compared to a threshold extracted from a χ^2-table corresponding to a false detection rate of 0.1%.

3.2.2 State Observer Approach using Adaptive Extended Kalman Filter

The state observer approach using AEKF is implemented and simulated in MATLAB, and depicted in Figure 3.2. The *Battery cell* is modelled using GSP. As explained in Section 3.3.2, real log data of battery load current from a FEV is used as input to the GSP battery cell model. Independent zero mean Gaussian noise is then added to both the current measurements, u_k, and the voltage measurements, y_k, in order to achieve realistic measurements in the simulation. Both the real log data and the simulated voltage measurements are then fed to the AEKF for estimation of internal states and generation of residual, according to Section 2.3.2. The model used in the AEKF for prediction and measurement update is the second order ECM presented in Section 2.2.2, where the temperature dependency of the parameters is fixed to $23°C$ and the coulombic efficiency is assumed to be one at all times, in order to simplify the model and decrease complexity. The effect of ageing is also neglected since the duration of the simulation time is much shorter than the duration needed for ageing effects to have significant effect on the parameter values. During the simulations the true initial state is set to $x_{0,true} = [0, 0, 0.5]^T$ in the system.

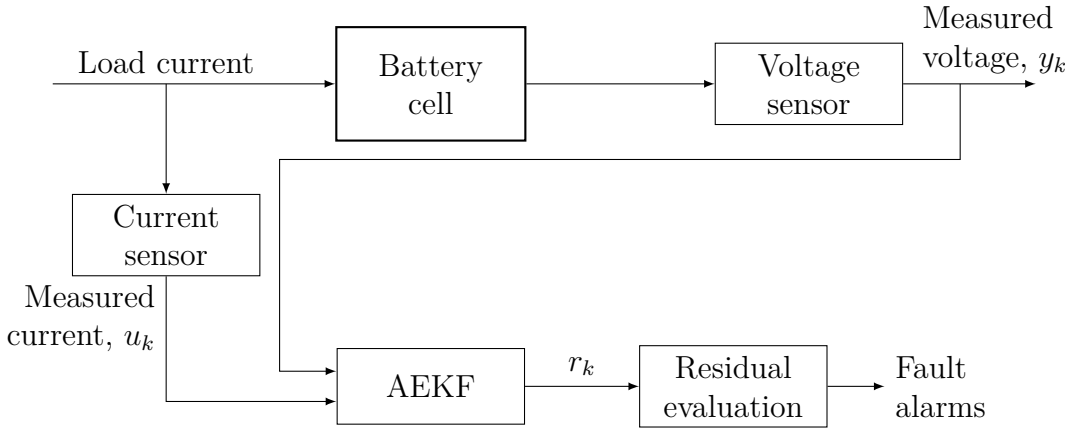

Figure 3.2: State observer approach with the Adaptive Extended Kalman Filter for fault detection in a battery cell.

3.2.2.1 Tuning of filter parameters

Tuning of the AEKF was performed by trial and error. The performance parameters taken into account when performing the tuning were residual sensitivity to errors, convergence speed of estimation, accuracy of SoC estimation, and insensitivity of the estimations to faults. The resulting initial mean, noise covariances and window size settings are presented in Table 3.4. The initial expected value of the SoC is set to be off by 10%, in order to test convergence speed of the filter. The initial error covariance for the SoC was chosen relatively large compared to the other two states to reflect the uncertainty in the initial state. The initial measurement noise covariance R_0 was set to the actual measurement noise covariance, σ^2, presented in Section 3.3.2. The initial process noise covariance for the SoC is chosen to be factor of 10^3 lower than the measurement noise, to reflect a high certainty in the

model. The initial process noise covariance as well as the initial error covariance for the other states is set to relatively small compared to the one for SoC in order for measurement updates to affect SoC rather than these transient voltages. The window size of sample covariance calculation is chosen so that it is large enough to estimate the covariance accurately and small enough to be able to reject sudden changes in the measurements i.e. faults.

Table 3.4: Initial mean, noise covariances and window size settings for AEKF simulations.

Parameter	Setting
x_0	$[0, 0, 0.4]^T$
P_0	diag($[10^{-20}, 10^{-20}, 10^{-3}]$)
Q_0	diag($[10^{-20}, 10^{-20}, 10^{-9}]$)
R_0	$1 \cdot 10^{-6}$
N	20

3.2.2.2 Evaluation of residual

Exactly as in Section 3.2.1.2 the fault-free samples of the generated residual signal are assumed to be independent zero mean Gaussian with variance corresponding to the measurement noise covariance. One can then construct a test statistic that follows the χ^2-distribution by taking the sum of squares of the residual from a window of N samples and normalising with the measurement noise covariance, which is presented in Equation 3.1.

$$w = r_{k-N+1:k}^T \; R_0^{-1} \; r_{k-N+1:k} \tag{3.1}$$

In this thesis it was found that this sum of squares corresponds to a scaled version of the sample covariance over window N, already calculated in the algorithm for update of noise covariances. One can receive the χ^2-statistic from the algorithm by multiplying the sample covariance with the window length and normalising with the known measurement noise. In order to test the null hypothesis, w is compared to a threshold extracted from a χ^2-table corresponding to a false detection rate of 0.1%. Since the degree of freedom of the statistic is dependent on the window size, so is the chosen threshold.

3.2.3 Injected faults during Battery Cell Detector simulations

The faults simulated for the PSA and AEKF method are foremost intended to emulate sensor faults but also process faults, such as parameter faults, are considered. Sensor faults that are injected during simulations are bias, drift and scaling faults added to the measurements of voltage and current. The internal resistance of the GSP battery cell model will be temporarily changed during simulations to see how

the system behaves when the model used in the AEKF differs from reality.

The magnitude of all injected faults is chosen relatively small compared to nominal values of measurements and parameters while still large enough for detection in order for simulation results to reflect near peak performance of the fault detection methods, i.e. to find how small errors can be detected. The fault detection schemes are assumed to be able to find all faults of the same type that is larger than these. For the AEKF method, larger faults are injected as well, in order to check the performance of the state estimation and the adaptation.

3.3 Test data

In this section information about the data used will be presented. The relevant measurements for this thesis includes voltage and current readings, which are taken with a specific sampling rate and accuracy. The communication over the CAN-bus affects the quality of the measurements. Since all of the units need to communicate over the same bus, packets containing measurements can be delayed due to that higher priority packets need the medium. This latency is determining the approximate update frequency with which measurements are received and available for calculations at the central computation unit. Since the information in the packets is represented by bits, the values that can be transmitted suffer to resolution limitations. Some units does not transmit direct measurements of voltage and current, but rather estimates of these quantities calculated from other measurements.

3.3.1 Logged data from full electric bus in operation

The data is provided by Volvo and consist of logged data under normal operation of the 55 route in Gothenburg between the 8^{th} to 10^{th} of January 2018. The specification of the data is shown in Appendix under Table A.1, where the estimated accuracy, approximate update frequency and resolution of the measurements from each unit are presented. The accuracy is calculated by estimating the sample covariance over a sequence where the measurements are constant. The sequences used are chosen such that the magnitude of the measurements are as high as possible while being stable over the period of estimation. The estimation of the covariance is done using the logged data and might not represent the accuracy over the entire measurement range, but gives an understanding of how the measurement compares to other readings in the system. All voltage accuracies are estimated around 630-635 V. The accuracy of the current measurements at the battery packs are estimated at 83 A, MDS at 47 A, DC/DC at 4 A and CSU at 343 A.

To be able to use the data in the Circuit Fault Detector, the data needs to be slightly altered. Nonconcurrent data can be handle but is not taken into account, instead the signals are re-sampled to have the same updating rate. In this case the updating frequency of 50 Hz is chosen, meaning that both the data from MDS and DC/DC needs to be down-sampled whereas data from CSU is up-sampled using zero order hold. The data used for the Circuit Fault Detector consist of 56 driving cycles and

64 charging cycles logged, as earlier mentioned, between the 8^{th} and 10^{th} of January 2018. The data are randomly divided into two equal sized sets of training data and validation data in order to train the thresholds.

The current readings from the MDS are not actual measurements, but are instead estimations from the AC measurements at the MDS. Hence the accuracy estimated will most likely be higher in reality. The same applies to the auxiliaries where the power consumption is estimated and sent on the CAN-bus. To find the approximate current consumption it is calculated using the TVS voltage at each specific time unit. Since no investigation in the actual estimation of the power consumption is done, the accuracy of the estimations cannot be properly estimated.

3.3.2 Simulated data for testing

The data used for both the AEKF and the PSA consists of both simulated and real logged data. The input to the system, the battery current, is logged from battery pack 1 during the FEV bus route 55 in normal operation during the 8^{th} of January 2018. The output of the system, the battery cell voltage, is on the other hand simulated using Volvo's Global Simulation Program (GSP). The GSP is developed to accurately simulate the characteristics of a battery cell. The battery specifications are for *City bus gen 2* and the details and parameters can be found at the Volvo GSP team.

For both the input and the output data noise is added to emulate measurement noise. The noise added for the input data is Gaussian zero mean with variance $\sigma^2 = 0.44$ A. This is derived by reviewing the market for current sensors in the automotive industry [13]. The noise added to the simulated cell output data is Gaussian, zero mean with a variance of $\sigma^2 = 1 \cdot 10^{-6}$ V. This is chosen by reviewing the market for *Lithium Ion Battery Monitoring Systems*, where three relevant variants where found. These three systems, two from *Analog Devices* and one from *Texas Instruments*, are ranging from ± 1.6 mV to ± 3 mV of accuracy [14][15][16]. The highest value of 3 mV is chosen with the assumption that the accuracy is for 3σ, i.e. 99.7 % probability that the measurement is within 3 mV from the true value. This gives a variance of $\sigma^2 = 1 \cdot 10^{-6}$ V.

4
Results

In this chapter the results of the implemented Circuit Faults Detector and Battery Cell Fault Detector are presented.

4.1 Circuit Fault Detector

During the testing of the Circuit Fault Detector it became evident that the residuals had different behaviour during driving and during stationary charging with an external charger. In Figure 4.1 residual, r_{u12}, is presented from a sequence containing both driving and changing cycles. In this figure it is possible to see that during driving the residual is zero mean indicating fault free behaviour, but during charging the residuals deviates significantly from zero surpassing the set threshold. This behaviour can be confirmed in all data sets used in this thesis. Because of this behaviour the driving and charging cycles will be handled separately regarding compensation constants, thresholds and filtering in order to enhance the detecting capabilities for each case. Charging performed by the MDS during driving is included as normal driving, and is not showing the same behaviour as an external charger.

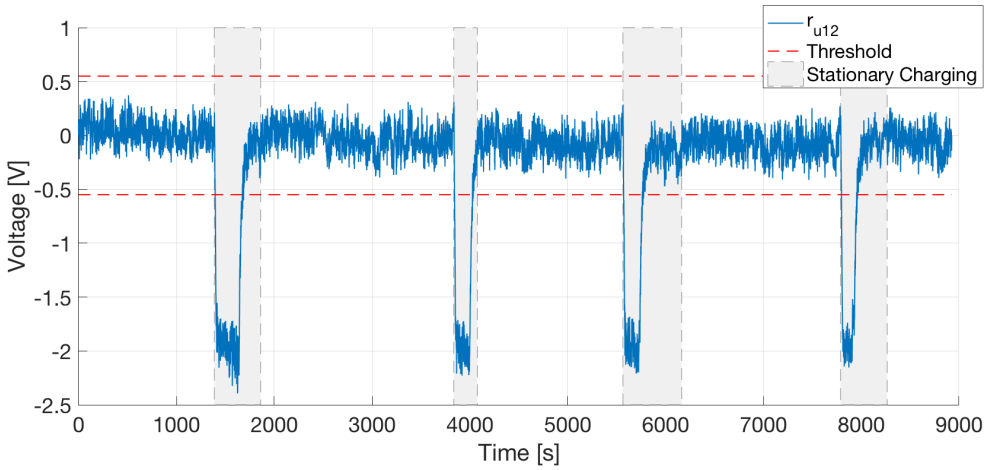

Figure 4.1: Residual r_{u12} from a sequence during 2018-01-08 containing both driving and charging cycles. The residual is deviating significantly during charging. The threshold is tuned for driving case and this shows how the detection capabilities can be enhanced if the driving and charging case are separated.

4.1.1 Tuning of bias compensation, thresholds and low-pass filters

As discussed earlier in the method the voltage measurements contains a bias and in Figure 4.2 this phenomenon can be observed, where the voltage from the four batteries are constantly biased compared to the MDS and among themselves. This has been detected in all log data used stretching from 2018-01-08 to 2018-01-12. By compensating for this bias the threshold is decreased and hence able to detect smaller faults in the system. The resulting compensation constants used during charging and driving is presented in Table 4.1.

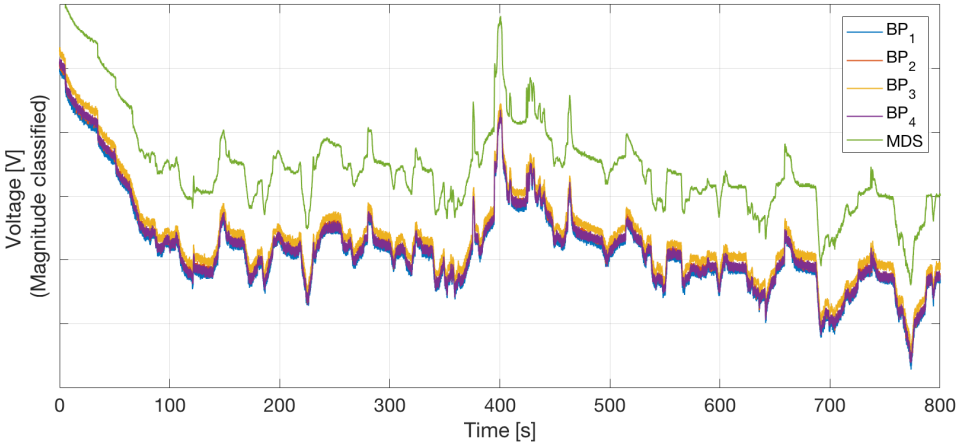

Figure 4.2: The voltage measurements contains a bias that can be seen in the measurements between the MDS and the the four battery packs. The batteries are also biased from each other.

Table 4.1: Constant added to the residuals to compensate for the bias in the measurements. They are tuned manually using the training data.

Constant	Charging [V]	Driving [V]
b_1	-6.05	-6.20
b_2	-2.90	-1.70
b_3	-6.00	-6.40
b_4	-2.60	-1.90
b_5	-4.50	-5.70
b_6	-0.75	-1.25
b_7	-5.30	-6.20

Constant	Charging [V]	Driving [V]
b_8	-1.60	-2.00
b_9	-0.50	0
b_{10}	-1.00	-0.40
b_{11}	-0.30	0.20
b_{12}	-0.50	-0.70
b_{13}	-0.20	0.10
b_{14}	0.50	0.85

The thresholds used for the detector were found by tuning using the training data to reach a low FDR. The thresholds were tested on the validation data to ensure that the threshold had not become overfitted to the training data. The resulting thresholds used for each residual can be seen in Table 4.2. The table includes the FDR for the specific threshold and the minimum fault magnitude one is able to deterministically detect. It is evident that it is possible to detect smaller faults in

the voltage residuals compared to the current residuals and the same holds for the driving case compared to the charging case.

Table 4.2: The resulting thresholds for each residual after training and the corresponding FDR on the validation data. The minimum magnitude of a fault required to deterministically detect the deviation in all scenarios is also presented for the residuals.

Voltage residuals						
	Charging			**Driving**		
Residual	Threshold	FDR	Min fault [V]	Threshold	FDR	Min fault [V]
r_{U1}	±1.7	0.0029	±3.4	±1.70	0.0015	±3.4
r_{U2}	±1.4	0.0001	±2.8	±0.90	0.0018	±1.8
r_{U3}	±1.8	0.0190	±3.6	±1.80	0.0018	±3.6
r_{U4}	±1.0	0.0011	±2.0	±0.90	0.0013	±1.8
r_{U5}	±1.4	0.0069	±2.8	±1.60	0.0111	±3.2
r_{U6}	±1.1	0.0001	±2.2	±1.00	0.0050	±2.0
r_{U7}	±1.5	0.0024	±3.0	±1.60	0.0078	±3.2
r_{U8}	±0.9	0.0002	±1.8	±1.20	0.0037	±2.4
r_{U9}	±1.3	0.0002	±2.6	±0.55	0.0037	±1.1
r_{U10}	±1.9	0.0012	±3.8	±0.75	0.0165	±1.5
r_{U11}	±1.7	0.0026	±3.4	±0.75	0.0076	±1.5
r_{U12}	±1.8	0.0013	±3.6	±0.55	0.0015	±1.1
r_{U13}	±1.8	0.0004	±3.6	±0.75	0.0021	±1.5
r_{U14}	±0.8	0.0010	±1.6	±0.40	0.0007	±0.8
Current residuals						
	Charging			**Driving**		
Residual	Threshold	FDR	Min fault [A]	Threshold	FDR	Min fault [A]
r_{i1}	±7.7	0.0189	±15.4	±7.7	0.0068	±15.4
r_{i2}	±1.2	0.0018	±2.4	±1.1	0.0048	±2.2
r_{i3}	±7.5	0.0030	±15.0	±4.0	0.0003	±8.0
r_{i4}	±6.2	0.0015	±12.4	±5.5	0.0010	±11.0
r_{i5}	±8.2	0.0001	±16.4	±4.0	0.0004	±8.0
r_{i6}	±6.3	0.0014	±12.6	±5.5	0.0010	±11.0
r_{i7}	±3.7	0.0064	±7.4	±2.0	0.0097	±4.0

The tuning of the low-pass filter affects the performance of the residuals significantly. The low-pass filter has two tasks, to suppress measurement noise and to suppress transients in the system. In Figure 4.3 a comparison between the filtered and unfiltered residual r_{i1} is presented where it is possible to see how the noise and transients are suppressed by the filter. The transients are a result of an abrupt change in the system not captured by the current estimations and measurements. It can be because of too low sampling frequency or inaccurate estimations. The transients arise only during driving and hence the low-pass effect of the filter used under charging can be relaxed to preserve more content of the original signals.

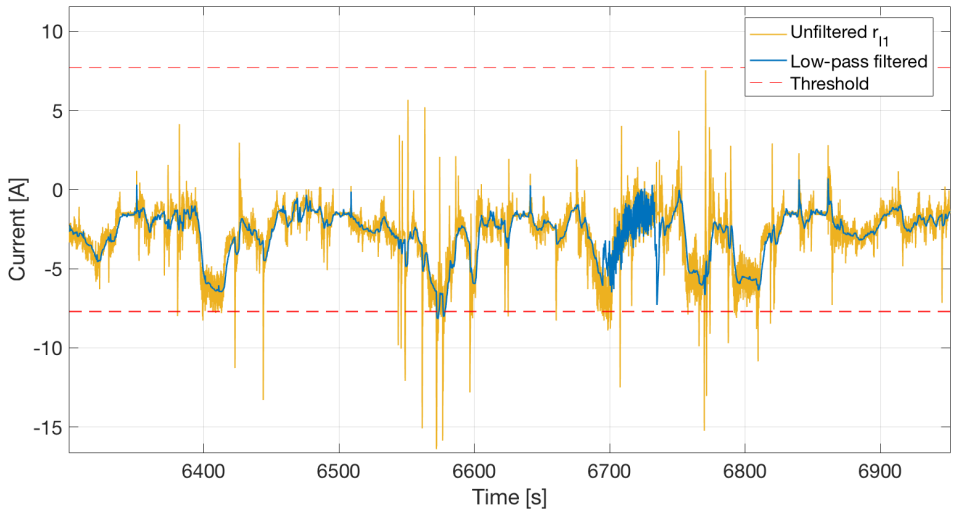

Figure 4.3: A comparison of the residual r_{i1}, filtered and unfiltered during driving. The filter is able to suppress the large transients and hence reduce the false detection. It can also be seen that the residual does not have zero mean, but rather -2.5 A.

Aside from the transients one can also notice that the residual has not a zero mean. It contains a bias and also patterns similar to square waves at certain positions. This behaviour can be explained by multiple reasons. The bias can be explained with uncalibrated sensors, giving a constant offset from the true value. The square wave patterns can be explained by the estimations being additionally inaccurate with higher current. The residual is constantly negative, meaning the batteries are measuring more current than the loads. This could mean that there is a load not being measured in the system.

One reason for the transients can be seen in in Figure 4.4, which is a comparison between the current measurements for the batteries and the estimated current from the MDS. As can be observed the signals are not synchronised in either time or magnitude during the entire sequence, where the current estimations from the MDS are ahead of the battery measurements. This happens when the MDS goes into a generative state and is charging the batteries. This gives that either the estimations or the sampling frequency of the measurements are not capturing the dynamics of the system, unless there exist a component taking care of the current peaks of the MDS generative state to protect the batteries.

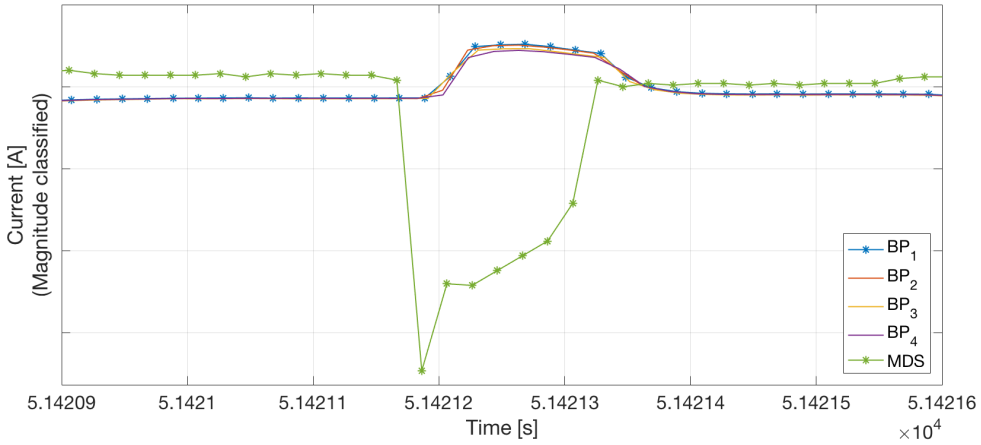

Figure 4.4: The current measurements of the batteries and the current estimations of the MDS. The estimation of the MDS current is not synchronised with the measurements in the batteries. This occur when the MDS goes into a fast generative state. The top value of the MDS is -173 A while the top value of the four batteries is 25.35 A.

4.1.2 Fault-free behaviour

First fault-free behaviour will be presented to provide the reader with understanding of how the implemented detector works, then an example of detection of an injected test fault will be shown.

The fault-free behaviour of the filtered current residual r_{i1} can be seen in Figure 4.3. One can notice that the residual does not have a zero mean and the noise is not the largest contribution to deviation. In Figure 4.5 residual r_{i5} is displayed showing the difference in the current measurements between two batteries. One can observe that these are not equal during neither charging or driving.

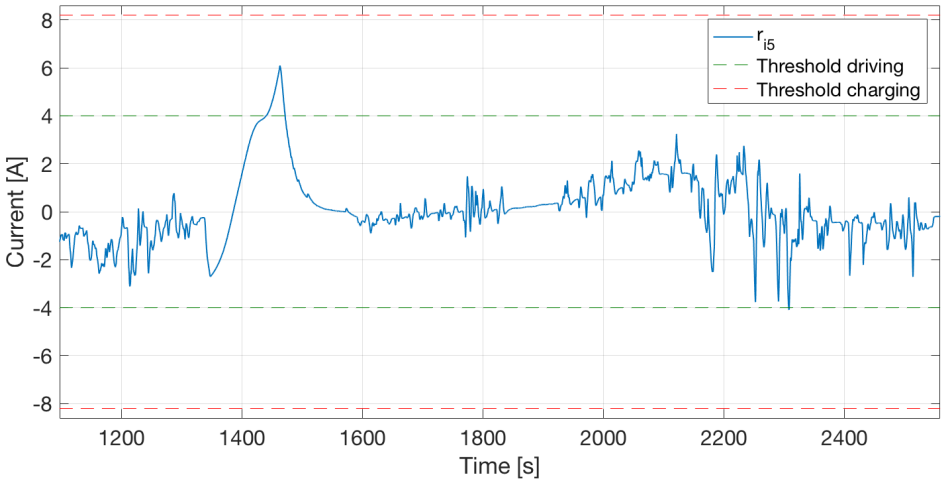

Figure 4.5: Current residual r_{i5} during both charging and driving. The current that flows in and out of the batteries diverge both during driving and during charging.

For the voltage residuals during driving the normal behaviour is zero mean with noise as the limiting factor for the threshold. This can be seen in the previously presented Figure 4.1. During charging the voltage residual is deviating from zero mean forcing the thresholds to be increased.

4.1.3 Fault detection performance

This section will provide an example of the Circuit Fault Detector detecting an injected fault during driving. The injected fault is a voltage drop at the DC/DC sensor of -3 V, which may represent a serial resistance fault. At the same time a current fault is injected as an increased current usage on each of the battery of 3 A with a total of 12 A, representing leakage current through a parallel resistance fault. The fault is injected into the validation data and in Table 4.3 the resulting MDR is presented. The voltage fault is clearly detected while the current fault has a MDR of 17 %. In Figure 4.6 two of the affected residuals are displayed.

Table 4.3: Results in form of MDR from the affected residuals in the voltage fault, -3 V at DC/DC, and the current fault, increased usage of +3 A at each battery pack.

Voltage residuals		
Residual	MDR	Total MDR
r_{U2}	0.007	0.006
r_{U4}	0.005	
r_{U6}	0.006	
r_{U8}	0.007	

Current residuals		
Residual	MDR	Total MDR
r_{i1}	0.170	0.170

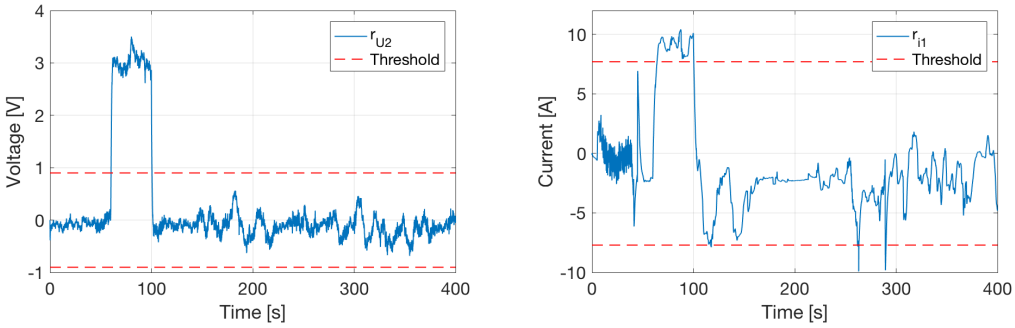

(a) Voltage fault in r_{U2}. **(b)** Current fault in r_{i1}.

Figure 4.6: The injected voltage fault of -3 V in the DC/DC is shown in figure (a) from the first driving cycle in the validation set. The injected current fault at each battery pack of 3 A is shown in figure (b) from the 28$^{\text{th}}$ driving cycle in the validation set. Both faults are active between $t = 60$ s to $t = 100$ s. The faults are in these sequences clearly detected by surpassing the threshold.

4.2 Battery Cell Fault Detector

In this section the results from both approaches will be presented, starting with the PSA and followed by the state observer approach using AEKF.

4.2.1 Parity Space Approach

In this section the results for Parity Space Approach will be presented, including behaviour of the linearised model, behaviour of the residual with and without fault present in the system.

4.2.1.1 Linearised model evaluation

In Figure 4.7 a comparison between the linear model and the nonlinear GSP is displayed for an operation cycle of 2.5 hours. One can notice that the linearised model deviates both during driving and charging. Temporarily the fast dynamics seems to be captured by the model but not in the entire sequence. One can also notice that there exists an error drift over time.

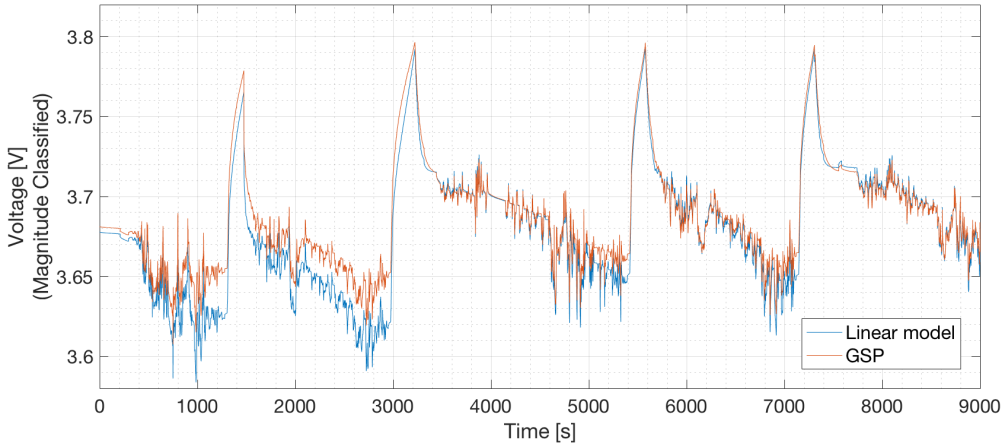

Figure 4.7: A comparison between the output of the GSP (nonlinear) and the linearised model used in the PSA. This figure does not contain measurement noise to show the models behaviour. The linearised model output diverge during both driving and charging. This sequence starts at a SoC of 50%.

4.2.1.2 Fault free behaviour

Before the faults are presented the fault free behaviour of the PSA is introduced in Figure 4.8. The first thing to note is that the residual gives a high reading during the four charging cycles. During driving the residual readings are significantly lower, but are still giving a relatively high reading compare to intended design, which should be close to zero.

The PSA residual turns out to not be zero mean and unit variance, meaning that it will not follow the χ^2 distribution and hence the distribution cannot be used to set a valid threshold. Instead of using this statistical approach of selecting a threshold, a nominal value of 2300 is chosen to give a FDR close to zero when disregarding the charging cycles.

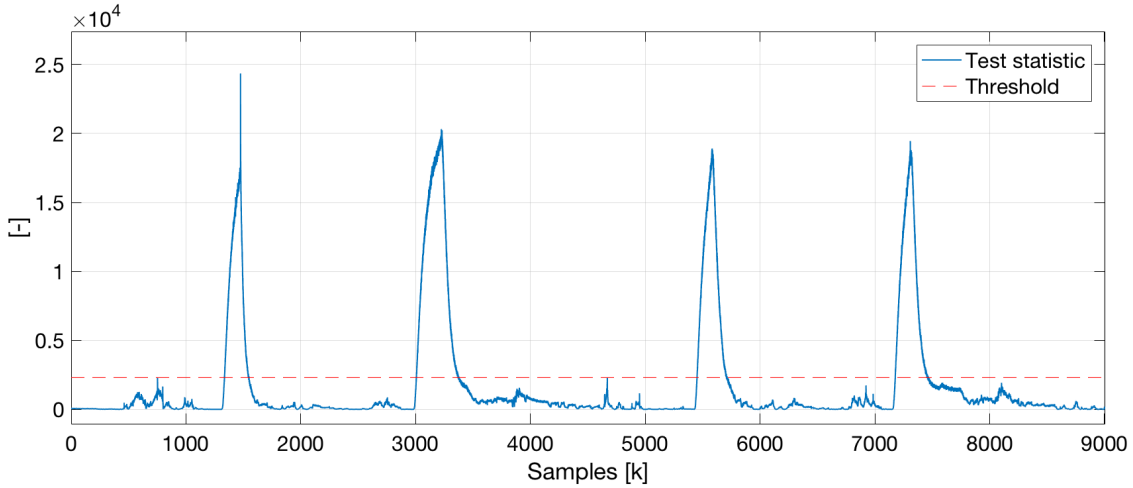

Figure 4.8: The fault free behaviour of the PSA with a nominal threshold value of 2300. One can notice the large discrepancies in the model during both charging and driving, since the residual should be close to zero during normal operation.

4.2.1.3 Fault detection performance

The faults discussed in Section 3.2.3 will in this section be injected to the Battery Cell Fault Detector when using PSA. Because of the significant model mismatch during charging the ability to detect faults when charging is not of interest, since model improvements are needed in order to use it. All faults will hence be injected during driving, except for the parameter fault.

In Figure 4.9, a bias fault is injected both in the voltage and current sensor. The voltage sensor fault is 50 seconds long and is started at $t = 2000$ s with a magnitude of 0.03 V. The current sensor bias fault is a 50 second fault injected at $t = 2100$ s with a bias of 25 A. Both the faults are clearly detected with no delay, the test statistic returns below the threshold as soon as the fault is over. Lower bias faults would not be fully detected.

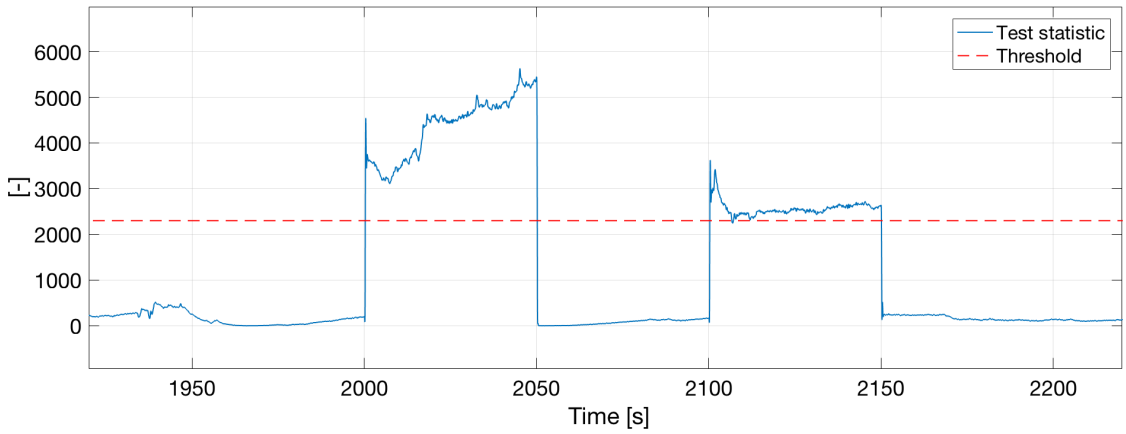

Figure 4.9: Resulting test statistic when injecting a 50 second 0.03 V bias fault in the voltage sensor at $t = 2000$ s and a 50 second 25 A fault in the current sensor at $t = 2100$ s. Both faults are exceeding the threshold and are hence detected.

In Figure 4.10 a drift fault is introduced in both sensors. For the voltage sensor a 50 seconds fault is started at $t = 4000$ s with a drift of $6 \cdot 10^{-4}$ V/s and for the current sensor a 50 second fault is started at $t = 4100$ s with a drift of 0.6 A/s. Both faults are eventually detected by the PSA, which is able to detect drift faults as long as the faults are large enough. One can note that the total accumulated drift for both the voltage and current sensor have almost the same value as the bias fault injected in the previous case. This gives that a delay will occur before the accumulated drift becomes larger than the set threshold.

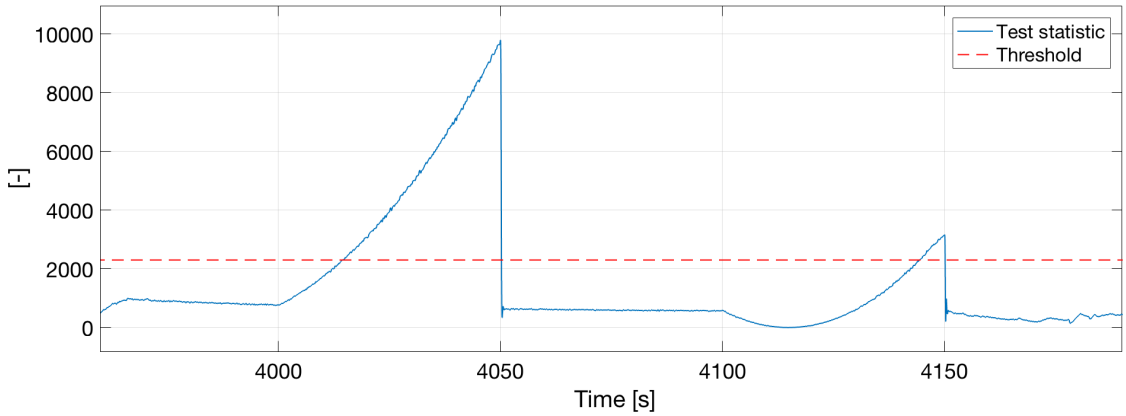

Figure 4.10: Resulting test statistic when injecting a 50 second drift fault of $6 \cdot 10^{-4}$ V/s in the voltage sensor starting at $t = 4000$ s and a 50 second drift fault of 0.6 A/s in the current sensor starting at $t = 4100$ s. Both faults are eventually detected when the fault becomes large enough.

In Figure 4.11 a 50 seconds scaling fault of 0.5% is starting at $t = 6000$ s for the voltage sensor, and a 50 second scaling fault of 100% is started for the current sensor at $t = 6100$ s. The scaling fault of the voltage sensor is detected without problem, while the scaling fault of the current sensor needs to be doubled before parts of the

fault can be detected. The difference between the two faults are the fluctuation in the input current, at times the current will be close to 0 A which will not be significantly affected by the scaling fault. The voltage measurements will always be around 3-4 V and will hence give close to the same fault regardless of which SoC state the system is in.

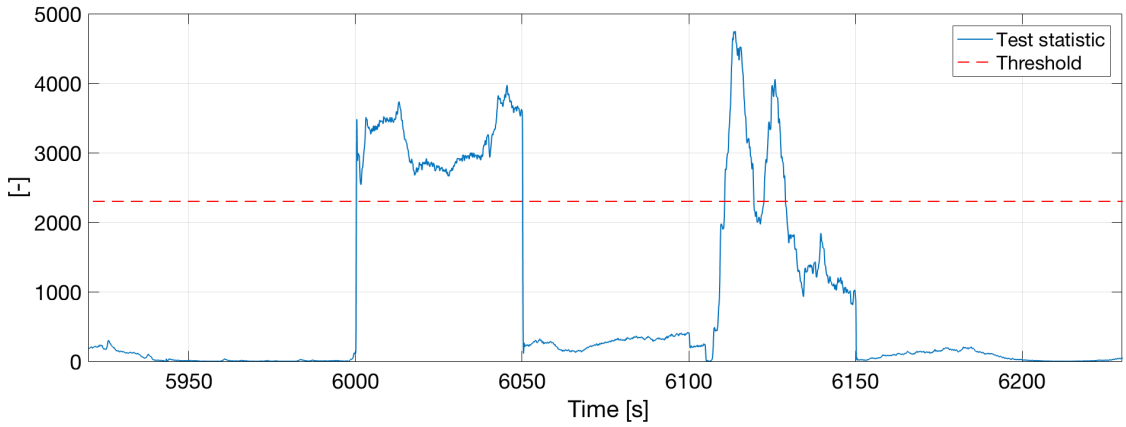

Figure 4.11: Resulting test statistic when injecting a 50 second 0.5% scaling fault in the voltage sensor at $t = 6000$ s and a 50 second 100% scaling fault in the current sensor at $t = 6100$ s. The voltage sensor fault is detected during the entire fault. The current sensor fault is only detected at certain instances when the input current is large enough to be affected by the fault scaling.

In Figure 4.12 the resulting test statistic from the PSA with a 50% increased internal resistance, R_0, is presented. The fault is injected at $t = 2600$ s and persists under 600 seconds, along with the test statistic for the fault free case. One can see that no fault is detected during driving between $t = 2600$ s and $t = 2980$ s. The fault can however clearly be seen during charging between $t = 2980$ s and $t = 3200$ s, when higher currents are flowing in the system. This parameter fault will be impossible to find during sequences with a low current, and easier to detect during higher currents since the output is directly affected by the input and the internal resistance, R_0. The observation can be made that this parameter fault behaves similarly as increasing the model mismatch of the system, which also is increased during higher current sequences.

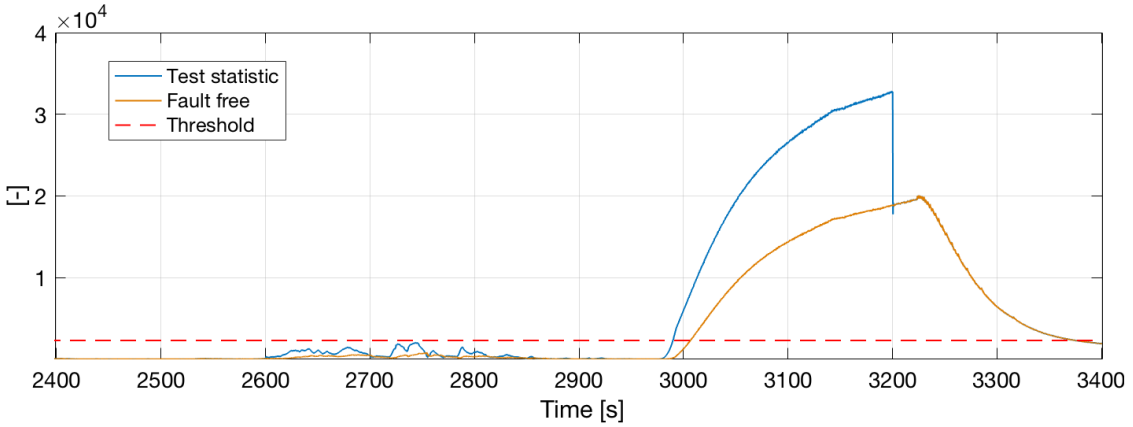

Figure 4.12: Resulting test statistic from the PSA when injecting a 600 second fault with an increased internal resistance of 50% at $t = 2600$ s. The fault is not detected initially, but it can be observed that when the current in the system increases the parameter fault can be detected.

4.2.2 State Observer Approach using Adaptive Extended Kalman Filter

In this section the results for the state observer is presented, including behaviour when no fault is present and when faults from Section 3.2.3 are injected in the system.

4.2.2.1 Nonlinear model evaluation

In order to check the accuracy of the nonlinear battery model used in the AEKF for prediction and measurement update, the output from GSP and the filter output from simulation are presented in Figure 4.13. Observe that they are simulated without noise and the initial filter parameters are set to correspond to the true state in GSP. Initial error noise and process noise are set very low, with adaptation turned off, in order for the filter to exclusively use the predicted value, i.e the model, without using measurement for estimation of posterior mean and covariance. One can notice an overall mismatch in the voltage, especially after charging at times $t = \{1500, 3300, 5600, 7400\}$ s but also during charging at the voltage peaks. The state estimates from the filter were also compared to the actual states from GSP. It was observed that the magnitude of the first two transient voltage states slightly mismatched while the SoC was found to follow GSP without errors.

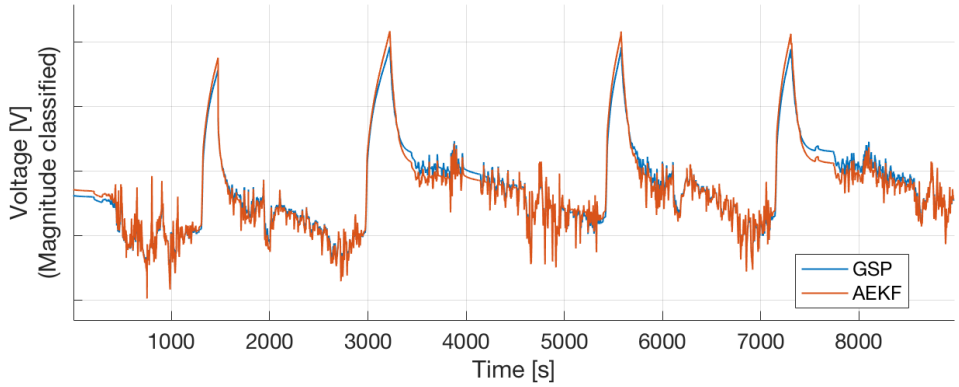

Figure 4.13: Output from GSP and AEKF simulation without added noise, when using only the model for posterior mean and covariance estimation in the filter.

4.2.2.2 Fault free behaviour of state and output estimation

In order to allow the reader to get an apprehension of normal, fault free, behaviour of the AEKF estimation of output and SoC, they are presented in Figures 4.14 and 4.15.

In Figure 4.14 measurements, true values from GSP and estimated output voltage from AEKF over a duration of approximately 1.5 minutes are presented. One can observe that the filter performs well in following the true output voltage. It is also able to follow fast transients of the system such at $t = 540$ s.

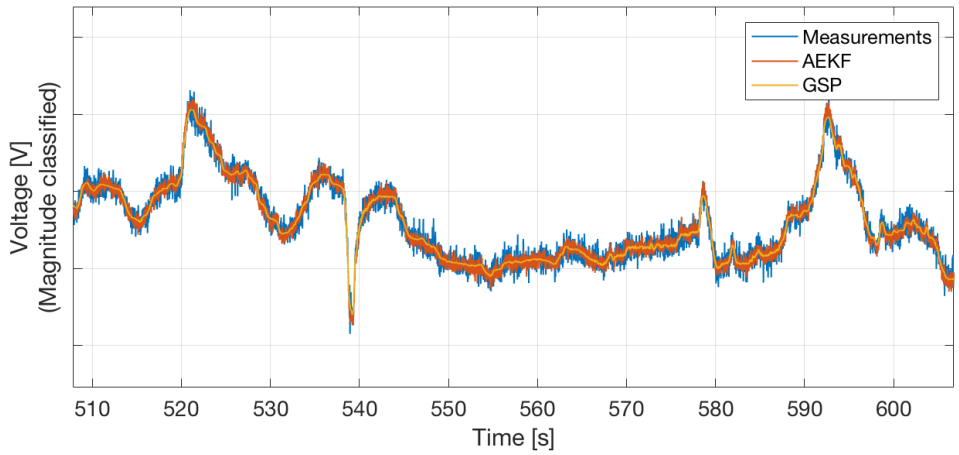

Figure 4.14: Measurements, true values from GSP and AEKF estimated output voltage corresponding to a fault free drive of approximately 1.5 minutes. One can observe that the filter performs well in following the true output voltage.

In Figure 4.15 the true values from GSP and estimated SoC are plotted. One can see that the maximum estimation error is about 1%. It should also be noted that these relatively larger errors occur after charging where the measurement model

mismatch as seen in Figure 4.14. The SoC estimation converges after just a couple of samples.

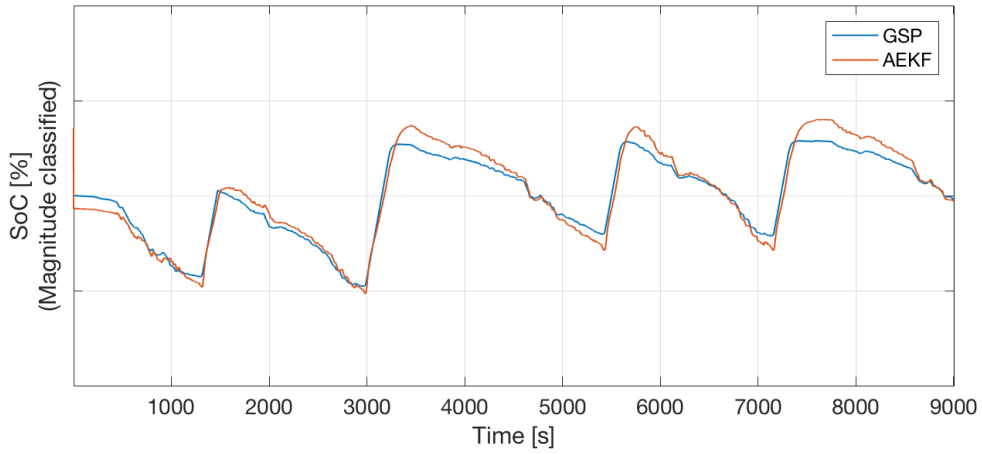

Figure 4.15: True values from GSP and AEKF estimates of SoC corresponding to a fault free drive of approximately 2.5 hours. One can see that the maximum estimation error is about 1%.

4.2.2.3 Fault detection performance

In Figure 4.16 the resulting χ^2-statistic when injecting a 50 second 0.015 V bias fault in the voltage sensor at $t = 2000$ s and a 50 second 5 A bias in the current sensor at $t = 2100$ s is presented. One can see that the two injected faults are clearly detected with very little delay for both sensors. One can also observe that after the fault injection, the χ^2-statistic returns to below alarm level. It was observed that for smaller values of the injected bias, the filter would adapt towards them, since the bias would not introduce enough change in the voltage residual to make the filter distrust the measurements.

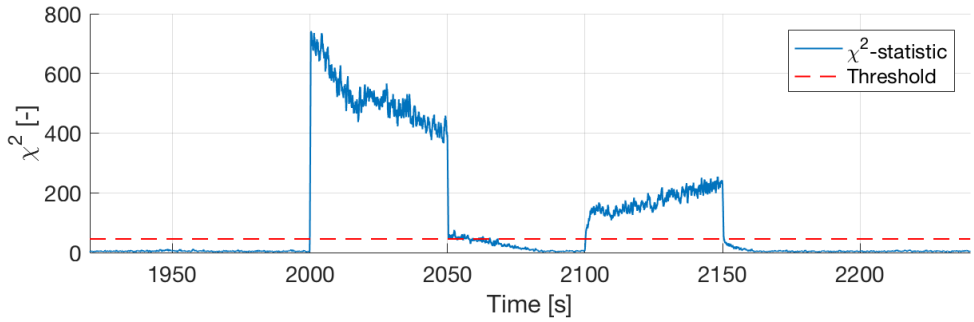

Figure 4.16: Resulting χ^2-statistic from the AEKF when injecting a 50 second 0.015 V bias fault in the voltage sensor at $t = 2000$ s and a 50 second 5 A bias in the current sensor at $t = 2100$ s.

In Figure 4.17 the resulting χ^2-statistic when injecting a 50 second $4 \cdot 10^{-4}$ V/s drift fault in the voltage sensor at $t = 4000$ s and a 50 second 0.004 A/s drift in the

current sensor at $t = 4100$ s is presented. The drift is well detected for both sensor types, after the divergence from the nominal value has grown large enough. The χ^2-statistic returns to below alarm level when the fault duration is over. The filter was not observed to adapt towards the fault for small divergences, as seen when injecting a small bias, as long as it experienced a fault with a non-zero rate of change.

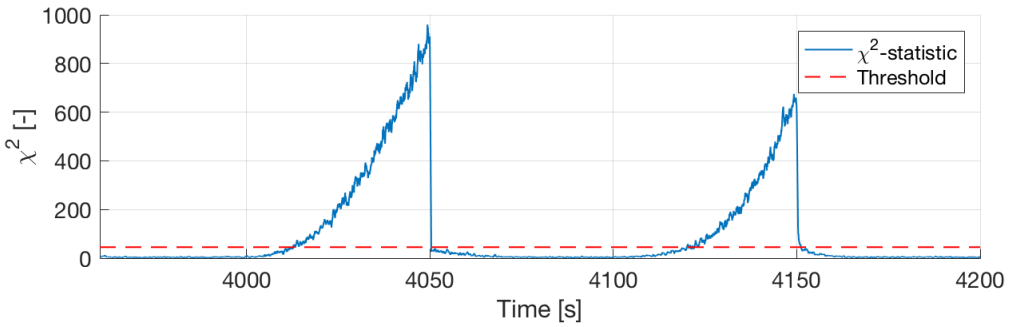

Figure 4.17: Resulting χ^2-statistic from the AEKF when injecting a 50 second $4 \cdot 10^{-4}$ V/s drift fault in the voltage sensor at $t = 4000$ s and a 50 second 0.004 A/s drift in the current sensor at $t = 4100$ s.

In Figure 4.18 the resulting χ^2-statistic when injecting a 50 second 0.25% scaling fault in the voltage sensor at $t = 6000$ s and a 50 second 30% scaling fault in the current sensor at $t = 6100$ s is presented. The scaling fault is detected for both sensors. The filter was observed to be more insensitive towards scaling faults in the current sensor, since the current, unlike the voltage, is zero frequently during operation.

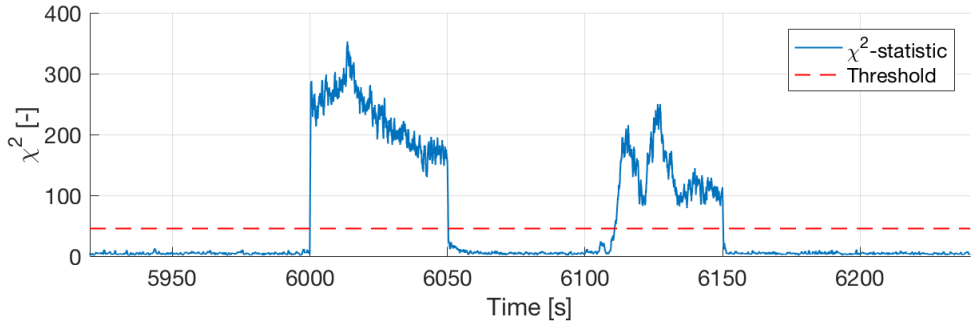

Figure 4.18: Resulting χ^2-statistic from the AEKF when injecting a 50 second 0.25% scaling fault in the voltage sensor at $t = 6000$ s and a 50 second 30% scaling fault in the current sensor at $t = 6100$ s.

In Figure 4.19 the resulting χ^2-statistic from the AEKF when injecting a 600 second scaling fault of 50% on the internal resistance, R_0 at $t = 2600$ s is presented. One can observe that some alarms arise between $t = 2600$ s and $t = 2980$ s, but the fault is mostly undetected during this time period. When the FEV goes into charging at $t = 2980$ s the fault is however clearly detected for a period of approximately

200 s. The χ^2-statistic is steadily decreasing during these 200 second until it is no longer detected. It should be noted that the scaling fault on R_0 is constant for the whole fault duration. When the fault is no longer injected at $t = 3200$ s, the χ^2-statistic grows large again and then decreases in a similar fashion as during charging.

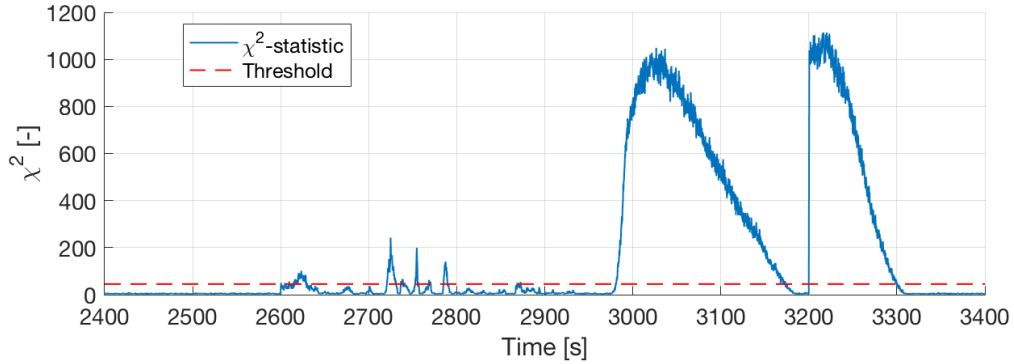

Figure 4.19: Resulting χ^2-statistic from the AEKF when injecting a 600 second scaling fault of 50% on the internal resistance, R_0 at $t = 2600$ s.

In Figure 4.20 the *SoC* estimation is plotted with and without adaption in the filter, with same fault signatures injected as presented above but with a small increase in magnitude in order highlight the performance of the adaptation. One can note that with adaptation the AEKF rejects the faults in the *SoC* estimation.

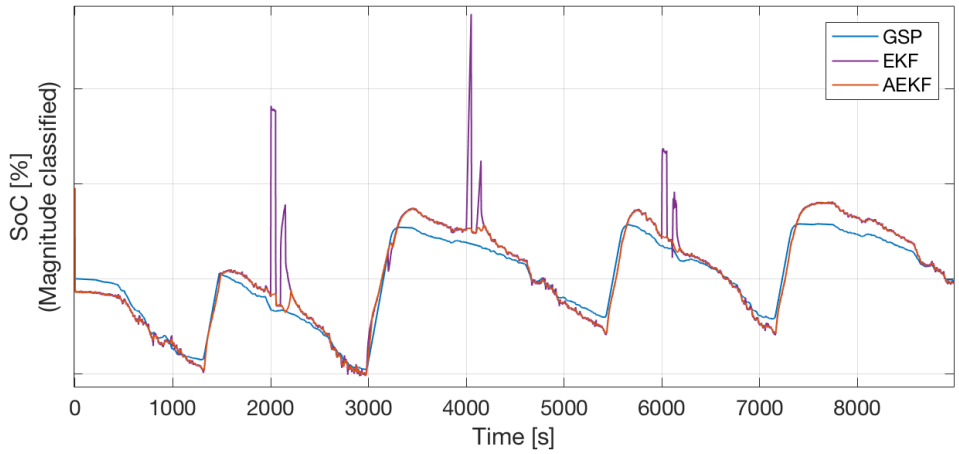

Figure 4.20: *SoC* estimation with (AEKF) and without (EKF) adaptation when injecting bias, drift and scaling faults in both current sensor and voltage sensor at different time instants.

5
Discussion

In this chapter the results from both the evaluation of the circuit detector and the battery cell detector are discussed.

5.1 Circuit Fault Detector

The circuit detector enable us to detect abnormalities in the TVS, if they are large enough. The thresholds are tuned with real logged data over three days of normal driving and should provide enough data to cover normal operation of the vehicle. The faults requested to be found are tested in the detector and shows expected results, they are found if the noise and dynamic deviations in the system are surpassed.

More research is recommended to be performed on why the current residual, r_{i1}, is not zero mean with the noise variance as the largest deviation. The behaviour of the residual points towards the dynamics in the system is not fully captured by measurements or estimations. This could be caused by the estimation of the auxiliaries. As shown in Figure 4.4 the current of the MDS and the batteries are not fully synchronised during fast transitions to generative state and since the currents in the system are typically high in these cases, it will result in large spikes in the residual. These large spikes severely degrade what is possible to achieve with the detector, since the threshold needs to be increased. A few techniques to circumvent this could be to low-pass filter the signals heavily, as is done in this implementation. Another method is to implement an rejection of short, few sampled alarms in the system, i.e. simply not send an alarm if the fault is shorter than a certain time limit. This could on the other hand be dangerous and lead to missed faults that are oscillating near the threshold. A third alternative is to disable the detector when the MDS is entering generative states.

The voltage residuals are designed based on the idea of an ideal system, where the source and load are having the same electrical potential. This is not applicable in a real implementation and hence constants are added to compensate. During the testing this approach seem to give good results, but the problem arise of how these constants should be tuned during operation. The bias is affected by the calibration of the sensors and the balance of the batteries. The bias in the signals was found to fluctuate up to 0.3 V depending on which day the data was logged. One method of correcting the bias could be to log the residuals over an amount of time, calculate the mean and update the compensation constants if necessary.

A shortcoming of the plausibility check is that it is not possible to distinguish if it is a process or sensor fault. Deviations will be detectable if large enough, but it is not possible to determine the nature of the fault. This is caused by process and sensor faults having the same effect on the residual, and the fact that a plausibility check have limited knowledge about the system behaviour. The designed detector is on the other hand able to locate which sensor or process in the system that is giving the inconsistent measurements. This is done by using the fault tree logic discussed in Section 3.1.1.

The low-pass filtering of the system is implemented to remove the large transients, which results in the detector responding slower to deviations. There is a trade off between how much the transients needs to be suppressed and how fast abnormalities can be detected. In this case the test faults were detected without noticeable delay, and will hence not affect detection of longer faults. Small oscillating faults might on the other hand be suppressed by low-pass filtering. In this method the Kalman Filter was used as a low-pass filter because the simplicity in the tuning. This is on the other hand a computational heavy method, and in an vehicle implementation a more efficient low-pass filter will be more feasible. This should not affect the actual performance as long as the filter is tuned properly in order to remove both noise and transients.

The Circuit Fault Detector can be improved in several different areas. The voltage sensors are performing well as is today, but can always be enhanced by improving both the frequency and the accuracy of the measurements. One can on the other hand argue that there are other areas in need of improvements before the voltage sensors. The current measurements should be enhanced in regard to sampling frequency and estimation. During testing it became evident that the operation of the MDS provides large transients in the current residuals during driving and that the residual is not zero mean, this points towards the sampling frequency or estimations is not capturing the full behaviour of the system. To conclude if it is the sampling frequency or the estimations in the system, a field test with proper measurement tools can be used to capture the correct behaviour of the current and compare it to the measurements by the installed sensors. The CSU is today using a frequency significantly lower than other measurements in the system, and since it is used to measure the high currents from the charger it has a great impact on the residual. It is also found to be the sensor with the worst accuracy.

In order to make sure the correct behaviour of the system is captured in the measurements, a high sampling frequency is needed and it should be investigated if the sampling frequency used today achieves this. Different sampling frequencies are used for different sensors in the system today, but only the lowest common frequency can be used in the detector and hence sensors with low frequency should be upgraded to increase the overall frequency in the fault detection. An increased sampling frequency may give rise to problems in the CAN-bus communication, which needs to be taken into account before an upgrade is carried out. Data communicated over

the CAN-bus can also give rise to synchronisation issues, hence the time stamp information in the communication packages should be used in order to avoid this problem. In a vehicle implementation the synchronisation should be evaluated in order to properly use the measured data.

Today certain areas of the TVS does not have measurements and hence these areas are not monitored by the detector. Examples are the three auxiliaries (heater, HVAC and air compressor) which today have no available voltage or current measurements at the used CAN-bus. The current can be calculated from the estimated power consumption, but provides no exact measurement. Increasing the measurement points in the system will provide the possibility for a more comprehensive fault localisation in the TVS.

Another approach to improve the fault detection capabilities is to use a more complex thresholding method, for example Adaptive thresholding. This could be used instead for the compensation constants added. It can also be used to increase the threshold when high currents are flowing, since the accuracy of the sensors usually are degraded.

It can be discussed if the threshold tuned for the six current residuals, r_{i2} - r_{i7} are relevant. Initially the residuals where designed to detect faults if the currents measured at the batteries deviated, but during testing it became evident that the batteries are in fact deviating in normal operation both during driving and charging. The currently tuned thresholds are set from the training data of 3 days of normal operation, but one can then ask the question how much the batteries should be allowed to deviate before it can be considered a fault, and instead tune the threshold according to this decided limit. These residuals are then monitoring how balanced the batteries are in the system and gives a warning if the batteries are too unbalanced.

A more comprehensive study of faults that can occur in the TVS and how they effect the system is recommended. This is important to do before a vehicle implementation since it then is possible to know if the faults could be detected with the designed detector or if improvements needs to be made. More importantly the study should conclude if the proposed improvements are cost effective in terms of the benefits these improvements would make, for example towards run time or preventive maintenance. It is hence important to know if the faults able to detect are necessary to find or if it is of no harm to the vehicle and would be repaired during the next service.

5.2 Battery Cell Fault Detector

From the results in Chapter 4.2 it became apparent that both methods of performing fault detection on a battery cell were able to detect different faults with some strengths and weaknesses. The AEKF did outperform the PSA in terms of magnitude of faults able to reliable detect with low FDR. A number of reasons have been considered for this such that the initial state is projected to null space in the PSA, which could potentially contain a lot of information of the fault signature. It was however observed that the PSA performed worse due to the model mismatch with the nonlinear battery cell model, where the threshold needed to be set higher to avoid false alarms.

The model of a battery cell presented in Section 2.2.2, was evaluated for both methods and it was found that there existed some model inconsistency between GSP and both the linearised model used for PSA and the nonlinear used for the AEKF. A first improvement that could be made is to remove the limitation mentioned in Section 3.2.2, that parameter values are used at a temperature of $23°C$. A more accurate model would include a temperature dependency and one could also model the ambient temperature in the cell as a dynamic state. Another improvement that could be done is to include ageing effects on the battery cell and track it using the so called state of health [17]. Over time the equivalent parameters in the battery cell will change through natural wear and tear. As the mismatch between the unchanged parameters in the model and the parameters in the cell increase over time, so does the test statistic and the amount of fault alarms, if not accounted for. Even though excluding ageing effects would not affect detectability or state estimation on the short time period used in this thesis, it would affect performance in a vehicle implementation where one expects the performance of the fault detection to stay within acceptable levels over periods of years. A sensible approach is to update model parameters as part of service of the vehicle or performing online parameter estimation from the measurements with some time interval, decreasing the need for an accurate ageing model. As one improves the model by including more dependencies and dynamics, one also increases the complexity. This could lead to problems with computations in a vehicle implementation. There is then a trade off between accuracy and complexity of the model. To be noted is that if the currently used model without improvement is found to be too complex, there exist potential solutions such as using a simpler first order battery cell ECM.

A natural future investigation would be how one could use methods as PSA and AEKF, which only performs fault detection in their current format, to perform fault isolation. Knowledge about where faults have occurred in the system is of great value as it allows the engineer to develop algorithms and functions to correctly react and adapt towards these faults. An approach is presented in [2], where one can isolate current and voltage sensor faults, assuming fault detection was performed on several battery cells. The fault signature for a current sensor would appear in the residual for every cell monitored, while a voltage sensor fault signature would only be seen in one of the residuals corresponding to the cell where the sensor

fault occurred. During the simulations it became apparent that the voltage sensor faults and parameter fault had similar behaviour, when looking at only one time instant. This could mean that one is not able to isolate voltage sensor faults from parametric faults, which impact is of different severity for the system and vehicle. It was observed however that the scaling error of R_0 had a certain fault signature, that would grow significantly during periods where the load current was high, and hence this behaviour showed especially during charging. According to [5] it is necessary to have multiple process outputs in order to perform fault isolation within only one process model. This is a drawback with the current model used for a lithium-ion battery cell, which only has one output.

5.2.1 Parity Space Approach

For the model now used in the PSA, the results show that the linear process model is lacking the capabilities of capturing the dynamics of the system over the entire range. It is important that the model used gives a good representation and the linear model is accomplishing that for a certain operating point, but are clearly not able to do it for the entire operation cycle. If one instead would disregard the model mismatch seen over the entire sequence in Figure 4.8 and only focuses on the sequences in Figure 4.9. Then one can observe that the threshold would be able to be lowered from 2300 to approximately 500 without any false detections and this would allow detection of lower faults. A way of improving the method could be to use a Linear Parameter Varying system model. This means the PSA would change the model parameters it uses during certain conditions, for example charging, and then better model performances could potentially be achieved. This does on the other hand result in a more complex method where multiple tuning of method parameters, such as W, needs to be performed. Improving the model as a solution to the entire range of the system does not seem as a feasible approach, since the battery cell has too nonlinear characteristics to be captured well enough by only one linear model. To further improve the system would be to implement an adaptive threshold method to follow the residual. This could for example be an increased threshold when higher currents are running through the system. More advanced adaptive threshold methods exists and are discussed in [6], this could be a solution instead of only improving the linear model.

The tuning of W in the PSA is not intuitive when using a single input single output system. When a multiple output system is at hand more freedom and more possibilities in the tuning to enhance certain faults can be performed. For an single output system the tuning possibilities is limited as well as the isolation of faults, since not enough information is delivered by the residuals. When tuning for the time horizon parameter q, no improvements could be found when it was increased. This might be because of the usage of a single input and single output system and the calculations of the test statistic, where the norm is taken of the residuals.

Since the PSA is using a linear model this method is not recommended for implementation as a fault detector in a lithium-ion battery cell. Improvements can be

made on several areas as discussed above, but approach methods that can handle non-linear models in a better fashion is instead recommended.

5.2.2 State Observer Approach using Adaptive Extended Kalman Filter

From the results in Section 4.2.2 it could be seen that the adaptation of process and measurement noise covariance both enable fault detection and makes the filter able to reject faults to retain normal state estimation even during the presence of faults. It was observed however that when faults where too small for detection or present for a longer time, as with the scaling fault on R_0, the filter started to converge towards the fault. This is an inevitable feature of the filter, since the filter is using measurements to a certain, although small extent even when errors are present. The increase of the test statistic after the parameter fault was no longer injected as can be seen in Figure 4.19, is a result of the fact that the filter has completely converged towards the fault and comprehend this as normal behaviour. When the fault duration is over, the filter register the change in measurements to actual normal behaviour as an abrupt fault signature. A way of mitigating completely converging towards a detected fault would be to turn of the adaptation when a fault has been present for a longer time, and only use the fault free current or voltage measurements, assuming one uses the approach for isolation suggested earlier. In this way one could potentially retain SoC-estimation capabilities with decreased accuracy for a while, but without fault detection capabilities. If an isolation of current sensor fault was made, the system could start using only the voltage measurements and the U_{oc} as a look up table for approximation of SoC. If a fault was isolated as voltage sensor or parameter fault, one could just use the current measurements and the model for SoC estimation by current integration but being susceptible towards drift of the estimation over time.

From the results in Section 4.2.2 it became apparent that even though a nonlinear model was used, there where model deficiencies of the second order ECM compared to GSP. Even though the prediction model of the SoC was very accurate, the inaccuracies in the model of the other two states as well as the measurement model ultimately led to some errors in the posterior mean of the SoC. The model inaccuracies could especially be seen after charging, and this combined with the adaptive part of the filter, would lead to a high residual and false alarms. After charging the value of measured voltage dropped fast, making the adaptive part of the filter react and increase the noise covariance for the measurement. The filter would then no longer follow the measurement as closely as before charging. Since the filter starts to distrust the measurements, it will trust the model to increased extent in a region where it is inaccurate. The mismatch between the measurements and estimated output i.e. the residual would grow, even though no fault was present. This behaviour is inherent to the Adaptive Kalman Filter, where large abrupt changes in the nominal system which is not captured by the prediction model, would cause an increased measurement covariance since the covariance of the residual would grow.This behaviour could be mitigated in several potential ways. Firstly the approach that was

used in this project, that one could tune the window size of the adaptation to be less sensitive to the fast natural change in the nominal system. The benefit of this approach are ideal since the filter retain its fault detection capabilities while not giving false alarms. This approach might however not always work since correct tuning depends on in what system the battery cell is used and the nominal behaviour of that system, and there is no clear rule in how to perform the tuning of the window size.

A second approach is to improve the actual model so that a mismatch between measurements and estimated output will not occur. False alarms would then no longer occur when the filter mostly trust the model in these critical regions. There are two potential limitations with this approach however, firstly reality versus model and secondly complexity, as discussed earlier. While one can improve the model a fair bit, to achieve a perfect description of reality is not reasonable. It should be noted that GSP used in the simulations in this thesis is just a more advanced model and that reality differ, so while a perfect model knowledge might be achieved in simulations, the model would still mismatch to reality. There is also the limitation of complexity, that as one extend the model to account for more physical laws, one increases the processing capabilities needed in order to calculate state transitions. According to [1], the recursive Kalman filter algorithm in itself is highly computation consuming, especially the calculation of the posterior error covariance. One should note that this detector is performing fault detection on a single cell, and when implemented in reality, one battery pack could contain hundreds of cells, making real time monitoring of them all unreasonable, especially if the model for each cell is very complex. A way of mitigating the problem of complexity when performing cell monitoring in a battery pack, is proposed in [3] where real time monitoring is performed on the two cells with highest and lowest output voltage since they are deemed to have the highest probability to be subjects to faults. Monitoring on the other cells is then performed in an offline fashion.

5.3 Limitation of theoretical faults

As mentioned previous, the faults injected during simulation of both the Circuit Fault Detector and the Battery Cell Fault Detector, where based on theoretical reasoning and claims from other sources such as [4]. A obvious drawback with this is that while the results are hinting towards a good performance of detecting faults, the faults in reality might behave differently than the ones simulated in this thesis. Without or limited knowledge of actual fault behaviour in the real system, the methods can only be evaluated to certain extent. Further on could more in depth knowledge of real fault behaviour and magnitude be used to tune each method to increase performance and also allow for isolation and identification of faults. The information of interest is the one that answers the following questions; what kind of faults can occur? Which are the most probable faults to occur? How do they affect the system? Which faults are relevant to detect and isolate?

6
Conclusion

In this chapter the specific questions under investigation are answered.

6.1 Circuit Fault Detector

In this thesis a plausibility method has been designed in order to detect abnormalities in the Traction Voltage System and one of the strengths is the easy implementation of the method. The method is proven to be suitable for detection but are on the other hand not as suitable to robustly isolate the faults. This is both due to the limitations in a plausibility test and that proper knowledge of the faults are missing. The resulting thresholds, presented in Table 4.2, gives the appropriate means of distinguish between normal and abnormal behaviour in the system as of today. The thresholds for the voltage residuals are limited by the covariance of the measurement noise while the thresholds for the current residuals are limited by ability to capture the dynamics in the current by the measurements and estimations performed today.

The key factors to improve for abnormality detection are estimations and measurements in the current residuals. The estimations and measurements are not capturing the dynamics well enough to provide a stable zero mean residual. By investigating if it is the measurements or the estimations that are degrading the performance of the current residuals, correct improvements can be made. To be able to monitor the entire system, addition of sensors to the auxiliaries is a necessity for full coverage of both voltage and current. In order to improve isolation, both the knowledge of faults and the addition of more residuals with the new measuring points at the auxiliaries are needed contributions.

Future work should contain a study of faults that can occur in the TVS and that are of interest to find, this would give insight if the proposed improvements are necessary and cost effective.

6.2 Battery Cell Fault Detector

Even if fault detection was achieved with the Parity Space Approach the results achieved are not good enough for proper implementation. The Parity Space Approach with a linear model does not have the capabilities to overall capture the dynamics of the nonlinear lithium-ion battery well enough, this weakness makes the method in its current form unsuitable to be used to monitor this system. The

strength lies in an easy implementation, but another weakness is how the tuning should be performed to enhance fault detection in a single input single output system.

The state observer approach using a AEKF performed well for the battery cell system, both at detecting faults and estimating SoC. The posterior SoC estimation is able to reject faulty sensor measurements by adaptation for a more accurate state estimation even during faults. A weakness of the method is, if faults are present for a longer time span, the filter converge towards the fault and it can no longer be detected. Potential problems could also arise with complexity of computation, due to extensive model and the algorithm computations if implemented in a FEV, when hundreds of cells need to be monitored simultaneously.

Future work should be done into actual fault signature of a battery cell and how to extend the fault detection algorithm to allow for fault isolation. An implementation in a FEV for further evaluation and development is also recommended for the AEKF. In a real implementation some re-tuning of filter parameters might be needed since the parameter set presented in this thesis is optimised towards GSP.

Bibliography

[1] S. X. Ding, *Model-Based Fault Diagnosis Techniques, Design Schemes, Algorithms and Tools*, 2nd ed. Springer, London, 2013. [Online]. Available: https://doi.org/10.1007/978-1-4471-4799-2.

[2] H. He, Z. Liu, and Y. Hua, "Adaptive extended kalman filter based fault detection and isolation for a lithium-ion battery pack", *Energy Procedia*, vol. 75, pp. 1950–1955, 2015, Clean, Efficient and Affordable Energy for a Sustainable Future: The 7th International Conference on Applied Energy (ICAE2015), ISSN: 1876-6102. DOI: https://doi.org/10.1016/j.egypro.2015.07.230. [Online]. Available: http://www.sciencedirect.com/science/article/pii/S1876610215009984.

[3] Z. Liu and H. He, "Sensor fault detection and isolation for a lithium-ion battery pack in electric vehicles using adaptive extended kalman filter", *Applied Energy*, vol. 185, pp. 2033–2044, 2017, Clean, Efficient and Affordable Energy for a Sustainable Future, ISSN: 0306-2619. DOI: https://doi.org/10.1016/j.apenergy.2015.10.168. [Online]. Available: http://www.sciencedirect.com/science/article/pii/S0306261915014105.

[4] E. Balaban, A. Saxena, P. Bansal, K. F. Goebel, and S. Curran, "Modeling, detection, and disambiguation of sensor faults for aerospace applications", *IEEE Sensors Journal*, vol. 9, no. 12, pp. 1907–1917, Dec. 2009, ISSN: 1530-437X. DOI: 10.1109/JSEN.2009.2030284.

[5] R. Isermann, *Fault-Diagnosis Systems, An Introduction from Fault Detection to Fault Tolerance*. Springer, Berlin, Heidelberg, 2006. [Online]. Available: https://doi.org/10.1007/3-540-30368-5.

[6] J. Chen and R. J. Patton, *Robust Model-Based Fault Diagnosis Dynamic Systems*. Springer, Boston, MA, 1999. [Online]. Available: https://doi.org/10.1007/978-1-4615-5149-2.

[7] F. Saidani, F. X. Hutter, R.-G. Scurtu, W. Braunwarth, and J. N. Burghartz, "Lithium-ion battery models: A comparative study and a model-based powerline communication", *Advances in Radio Science*, vol. 15, pp. 83–91, 2017. DOI: 10.5194/ars-15-83-2017. [Online]. Available: https://www.adv-radio-sci.net/15/83/2017/.

[8] S. Thanagasundram, R. Arunachala, K. Makinejad, T. Teutsch, and A. Jossen, "A cell level model for battery simulation", Nov. 2012.

[9] S. Li and X. Cheng, "A comparative study on rc models of lithium-ion battery", in *2014 IEEE Conference and Expo Transportation Electrification Asia-Pacific (ITEC Asia-Pacific)*, Aug. 2014, pp. 1–4. DOI: 10.1109/ITEC-AP.2014.6940818.

[10] A. H. Mohamed and K. P. Schwarz, "Adaptive kalman filtering for ins/gps", *Journal of Geodesy*, vol. 73, no. 4, pp. 193–203, May 1999, ISSN: 1432-1394. DOI: 10.1007/s001900050236. [Online]. Available: https://doi.org/10.1007/s001900050236.

[11] J. J. Gertler, *Fault detection and diagnosis in engineering systems*. CRC Press, 1998, ISBN: 0824794273.

[12] E. DePoy and L. N. Gitlin, "Chapter 20 - statistical analysis for experimental-type designs", in *Introduction to Research (Fifth Edition)*, E. DePoy and L. N. Gitlin, Eds., Fifth Edition, St. Louis: Mosby, 2016, pp. 282–310, ISBN: 978-0-323-26171-5. DOI: https://doi.org/10.1016/B978-0-323-26171-5.00020-3. [Online]. Available: https://www.sciencedirect.com/science/article/pii/B9780323261715000203.

[13] LEM. (2017). Datasheet: Automotive current transducer open loop technology hah1bvw s/04, [Online]. Available: https://www.lem.com/sites/default/files/products_datasheets/hah1bvw_s04_public_datasheet.pdf.

[14] Analog Devices. (2011). Datasheet: Lithium ion battery monitoring system: Ad7280a, [Online]. Available: http://www.analog.com/media/en/technical-documentation/data-sheets/AD7280A.pdf.

[15] ——, (2018). Datasheet: Lithium ion battery monitoring system: Ad7284, [Online]. Available: http://www.analog.com/media/en/technical-documentation/data-sheets/ad7284.pdf.

[16] Texas Instruments. (2010). Datasheet: 3 to 6 series cell lithium-ion battery monitor and secondary protection ic for ev and hev applications: Bq76pl536, [Online]. Available: http://www.analog.com/media/en/technical-documentation/data-sheets/ad7284.pdf.

[17] Y.-H. Chiang, W.-Y. Sean, and J.-C. Ke, "Online estimation of internal resistance and open-circuit voltage of lithium-ion batteries in electric vehicles", *Journal of Power Sources*, vol. 196, no. 8, pp. 3921–3932, 2011, ISSN: 0378-7753. DOI: https://doi.org/10.1016/j.jpowsour.2011.01.005. [Online]. Available: http://www.sciencedirect.com/science/article/pii/S0378775311000772.